UNIVERSITÀ DEGLI STUDI DI PADOVA

UNIVERSITA' DEGLI STUDI DI PADOVA

Department of Industrial Engineering DII

Master's Degree in Energy Engineering

Development of a test protocol for particle tracking velocimetry of turbine wakes in a towing tank

Supervisor: Prof. Giorgio Pavesi

Co-supervisor: David Roger Lande-Sudall

Student

(Ehsan Davoudabadifarahani, 2043073)

Academic Year 2024/2025

Contents

1. Abstract 4

2. INTRODUCTION 8

2.1. Background and geometry 19

2.2.Background Theory 25

2.3. Key Concepts and Equations 26

2.4. Blade Element Momentum (BEM) Theory 27

2.4.1. Principles of BEM Theory 27

2.4.2. Corrections and Extensions 29

2.4.3.Reynolds Number 29

2.5 Characteristics of Turbulent Wake 30

3. Methodology 31

3.1. Lagrangian Flow 31

3.2. Installation of the PIV System 32

3.3. Experimental Procedure 39

3.4. Particle Injection and Turbulence Generation 43

3.5. Improved Particle Injection Method 48

3.6. Final Particle Injection Method 50

4. Results 53

4.1. Flow Field Measurements 53

4.2. Velocity Field Analysis at Mid-depth 54

4.3 Turbulent Kinetic Energy (TKE) Development 54

4.4 Influence of Seeding Technique 55

4.5. Diagrams 57

4.6. Vorticity Distribution Analysis 60

4.7. Deficit Distribution at 1D, 2D, and 4D 61

4.8. Effect of Seeding Strategy on Wake Quality 61

4.9. Near-Wake TI and Vortex Signatures at z_1 63

4.10. Vorticity Distribution and Blade Tip Shedding 64

4.11. Seeding Effects and Flow Visualization Quality 66
5. Discussion 68
5.1 Wake Structure and Momentum Deficit Behavior 68
5.2. Turbulent Kinetic Energy and Tip Vortex Breakdown 68
5.3.Influence of Nacelle Geometry on Wake Development 69
5.4. Synthesis of Results and Theoretical Context 71
6. Conclusion 73
7. Suggestions for the Future Work 74

1. Abstract

The advancement of sustainable energy systems increasingly depends on optimizing the efficiency of turbine-based technologies, including wind and tidal energy converters. A fundamental component of this optimization lies in the detailed understanding of wake dynamics—the complex flow behavior downstream of turbine rotors. This thesis presents a comprehensive experimental investigation into the near and intermediate wake characteristics of a horizontal-axis turbine using high-resolution Particle Image Velocimetry (PIV) in a controlled towing tank environment. The experiments were conducted at MarinLab, HVL Bergen, employing a customized turbine rotor (D = 0.7 m) with NACA 633-418 airfoil blades, operating at an inflow velocity of 0.8 m/s and under strictly controlled seeding conditions.

The PIV measurements were performed at three downstream positions (1D, 2D, 4D) and three vertical planes (z_1, z_2, z_3), using a multi-camera “Shake-the-Box” configuration, enabling time-resolved velocity field reconstruction. Three seeding strategies were examined to evaluate their effect on flow visualization quality and data fidelity. Rinse-aid premixed particles provided the most reliable seeding, ensuring homogeneity and high signal-to-noise ratio in recorded images. Detailed analysis of the streamwise velocity, turbulence intensity, vorticity, and turbulent kinetic energy (TKE) was performed at each measurement plane.

Results showed a significant velocity deficit at 1D downstream, with progressive recovery at 2D and 4D due to enhanced entrainment and mixing. Vorticity fields revealed strong blade-tip vortices in the near wake, which decayed and diffused downstream, transitioning to more homogeneous turbulence. TKE distributions peaked at the rotor tip shear layer and decayed with downstream distance, consistent with wake diffusion theory. Depth-wise comparisons further highlighted mid-plane symmetry and stronger flow resolution at z_2, while deviations at z_1 and z_3 were linked to tank boundary effects and nacelle interactions.

This work contributes to the development of PIV-based protocols for characterizing turbine wakes in experimental towing tanks. The findings serve as a validation benchmark for numerical models and offer insight into rotor-wake interactions critical

for optimizing turbine design and spacing in array configurations. Additionally, the results underscore the importance of seeding strategy and experimental resolution in accurately capturing coherent flow structures and wake recovery phenomena. These insights support future turbine development in both wind and tidal energy applications.

Nomenclature

Symbol	Description	Unit
D	Rotor diameter	m
R	Rotor radius (R=D/2)	m
U_∞	Freestream inflow velocity	m/s
u,v,w	Velocity components in streamwise, vertical, transverse directions	m/s
$\bar{u}$	Mean streamwise velocity	m/s
u′,v′,w′	Velocity fluctuations (turbulent components)	m/s
ω	Rotor angular velocity	rad/s
ωz	Out-of-plane vorticity	1/s
ΔU	Velocity deficit	m/s
TI	Turbulence Intensity	–
TKE	Turbulent Kinetic Energy	m^2/s^2
λ	Tip Speed Ratio	–
C_T	Thrust coefficient	–
C_P	Power coefficient	–
μ	Dynamic viscosity	Pa·s
ρ	Fluid density	kg/m^3
ν	Kinematic viscosity	m^2/s
Re	Reynolds number	–

List of Abbreviations

Abbreviation	Full Form
PIV	Particle Image Velocimetry
STB	Shake-the-Box (volumetric particle tracking algorithm)
TKE	Turbulent Kinetic Energy
TSR	Tip Speed Ratio
ADV	Acoustic Doppler Velocimetry
CFD	Computational Fluid Dynamics
LED	Light Emitting Diode
FOV	Field of View
RMS	Root Mean Square
ROI	Region of Interest
NaN	Not a Number (invalid value in PIV processing)
SNR	Signal-to-Noise Ratio
DoF	Degrees of Freedom
PTV	Particle Tracking Velocimetry
PPM	Particles Per Million (concentration)

2. INTRODUCTION

The pursuit of sustainable energy sources has led to the critical exploration of offshore wind energy. Wind power has been harnessed for centuries, with early societies utilizing windmills for various tasks like grinding grains and pumping water. However, the development of offshore wind turbines as we know them today came about later, evolving from onshore wind turbine technology[1].

In recent years, offshore wind turbines have become increasingly popular due to the advancements in technology and engineering that allow us to tap into the vast wind resources available at sea. Interestingly, the concept of generating wind energy offshore was first explored in the 1970s with the installation of the Vindeby turbine off the coast of Denmark. Although it only had a capacity of 450 kW, it served as a valuable starting point for the development of the larger and more efficient turbines that we use today[1].

impressive renewable energy portfolio. This growth shows no signs of slowing down, with further expansion planned in both Europe and beyond[2].

From the initial days of the Vindeby turbine, offshore wind technology has made remarkable progress, powered by technological advancements and policy backing. Countries in Europe, particularly those around the North Sea, have led the way in offshore wind advancement, motivated by ambitious renewable energy goals and favorable coastal wind conditions. The United Kingdom has established itself as a forerunner in offshore wind capacity, with projects like the London Array and Hornsea Wind Farm playing a significant role in the country's impressive renewable energy accomplishments. This progress is poised to continue with future expansion plans in Europe and other regions[2].

As offshore wind technology advanced, turbines became larger and installations moved further from shore into deeper waters. This expansion presented new obstacles, including engineering, logistics, and environmental impact assessments. To surmount these challenges and unlock the vast potential of offshore wind in deeper waters, innovative solutions have been developed, such as floating offshore wind platforms and advanced foundation designs[3].

Despite its rapid growth, the offshore wind industry still faces obstacles, such as the intermittency of wind resources, grid integration, and cost competitiveness with other forms of energy generation[4]. Nevertheless, ongoing research and development initiatives, coupled with supportive government policies and declining costs, are powering continued growth and innovation in the sector.

The study of offshore wind farms is a multifaceted field that encompasses a diverse range of research areas. This includes exploring the aerodynamics and structural engineering of wind turbines, evaluating environmental impacts, and assessing how these turbines can be integrated into existing power grids. Over the years, many studies have been conducted to unravel the complex interplay between wind turbines, their surroundings, and the various stakeholders involved in offshore wind energy development.[5]

Initially, research efforts centered around the efficiency and dependability of singular wind turbines, intending to refine their design and usage to achieve optimal energy output. Such studies served as a basis for the advancement of offshore wind farms, showcasing the viability and promise of utilizing wind power in marine environments[6].

With advancements in offshore wind technology, the focus has shifted towards optimizing wind farm layout and configuration. The goal is to increase energy yield while minimizing environmental impacts and wake effects. Computational modeling and simulation techniques, including computational fluid dynamics (CFD) and wake modeling, have been instrumental in predicting and analyzing wind farm behavior in varying operating conditions[7].

In recent years, there has been a growing emphasis on examining the socio-economic factors surrounding offshore wind energy. This includes analyzing how it affects nearby communities, job opportunities, and overall economic growth. Policymakers and stakeholders must comprehend the wider socio-economic effects of offshore wind farms to make well-informed choices when it comes to project development and investment[7].

In recent times, the domain of offshore wind farm analysis has witnessed a remarkable expansion, thanks to the steady progress in technology and research methodologies In recent times, various remote sensing technologies, such as LiDAR (Light Detection and Ranging) and satellite imagery, have emerged as prominent tools for assessing

wind resources, monitoring turbine performance, and conducting environmental surveys. These technologies have proven to be particularly useful, owing to their ability to provide accurate and reliable data from remote locations, thereby facilitating better decision-making processes in the field of wind energy[8].

Furthermore, in recent years, it has become more common to take an interdisciplinary approach to studying offshore wind farms, which involves combining engineering, environmental science, economics, and policy analysis. This holistic approach is crucial for tackling the complex challenges and opportunities associated with offshore wind energy development[9].

The exploration of offshore wind energy in pursuit of sustainable energy sources has led to remarkable advancements in technology and engineering, enabling us to access vast wind resources available at sea. Early societies harnessed wind power through windmills for various tasks, such as grinding grains and pumping water. However, the development of offshore wind turbines as we know them today evolved from onshore wind turbine technology[10].

Recent years have seen an increasing popularity in offshore wind turbines due to advancements in technology and engineering, with the concept of generating wind energy offshore first explored in the 1970s with the installation of the Vindeby turbine off the coast of Denmark. Although it only had a capacity of 450 kW, it served as a valuable starting point for the development of the larger and more efficient turbines in use today[10].

Countries in Europe, particularly those around the North Sea, have led the way in offshore wind advancement, motivated by ambitious renewable energy goals and favorable coastal wind conditions. The United Kingdom has established itself as a forerunner in offshore wind capacity, with projects like the London Array and Hornsea Wind Farm playing a significant role in the country's impressive renewable energy accomplishments. This progress is poised to continue with future expansion plans in Europe and other regions.

As offshore wind technology advanced, turbines became larger, and installations moved further from shore into deeper waters. This expansion presented new obstacles, including engineering, logistics, and environmental impact assessments. To surmount these challenges and unlock the vast potential of offshore wind in deeper

waters, innovative solutions have been developed, such as floating offshore wind platforms and advanced foundation designs[11].

Despite its rapid growth, the offshore wind industry still faces obstacles such as the intermittency of wind resources, grid integration, and cost competitiveness with other forms of energy generation. Nevertheless, ongoing research, development initiatives, coupled with supportive government policies and declining costs, are powering continued growth and innovation in the sector[11].

In addressing the development of test protocols for Particle Tracking Velocimetry (PTV) of turbine wakes in a towing tank, it is essential to consider the broader context of wind energy research and its critical challenges. According to Veers et al. (2019), the advancement of wind energy technology is paramount to meeting the growing global demand for clean energy. Wind energy, with its zero-cost fuel and low life-cycle pollutant emissions, has the potential to become a major source of electricity. However, this potential can only be realized through significant innovations in several key areas[12].

Veers and colleagues identify three grand challenges in wind energy research that are particularly relevant to the study of turbine wakes. Firstly, there is a need for a deeper understanding of the physics of atmospheric flow within wind power plant operation zones. Characterizing the wind power plant operating zone in the atmosphere is essential to designing the next generation of larger wind turbines and achieving dynamic control of these machines. Improved atmospheric flow modeling will enable enhanced forecasting of atmospheric inflow, which is crucial for controlling the plant to support the grid effectively. This understanding is crucial for designing more efficient and larger wind turbines and for achieving dynamic control of these machines[12].

Secondly, advancements in the materials and system dynamics of wind turbines are necessary to improve their efficiency, durability, and cost-effectiveness. The materials used in turbine construction and the dynamic behavior of these large, rotating machines require innovative engineering solutions to enhance performance and reduce costs. Larger rotor diameters and higher hub heights, coupled with more efficient blade designs and better materials, contribute to significant reductions in the levelized cost of energy (LCOE)[12].

Thirdly, optimizing and controlling fleets of wind plants, which consist of numerous individual turbines working synergistically within the larger electrical grid, is essential for maximizing their contribution to the electricity supply. This optimization requires sophisticated control systems that can manage the variability and uncertainty inherent in wind energy generation. These systems must integrate advanced computational models and data analytics to ensure the reliable and efficient operation of wind plants within the electrical grid.

These challenges underscore the importance of interdisciplinary research and innovation. Enhanced atmospheric flow modeling, for instance, can lead to better turbine designs and control strategies, while advancements in materials science can enhance turbine performance. Additionally, improved forecasting and control systems are vital for integrating wind power into the grid effectively. The interdependence of these challenges requires an integrated approach, where progress in one area supports advancements in the others.

Accurately characterizing the wake dynamics of wind and tidal turbines is essential for optimizing turbine design and improving the performance of energy systems in multi-turbine environments. Particle Image Velocimetry (PIV) provides a non-intrusive, high-resolution technique for capturing the velocity field and turbulence structures within turbine wakes. Developing reliable and repeatable PIV test protocols is therefore critical to understanding the complex flow interactions that govern wake recovery, vortex shedding, and turbulence generation. This thesis contributes to that effort by refining PIV methodology in a towing tank environment and analyzing wake characteristics at multiple downstream positions and depths. The results offer valuable insight into the behavior of turbine wakes, supporting the advancement of turbine layouts and array configurations in future wind and marine energy applications.[12].

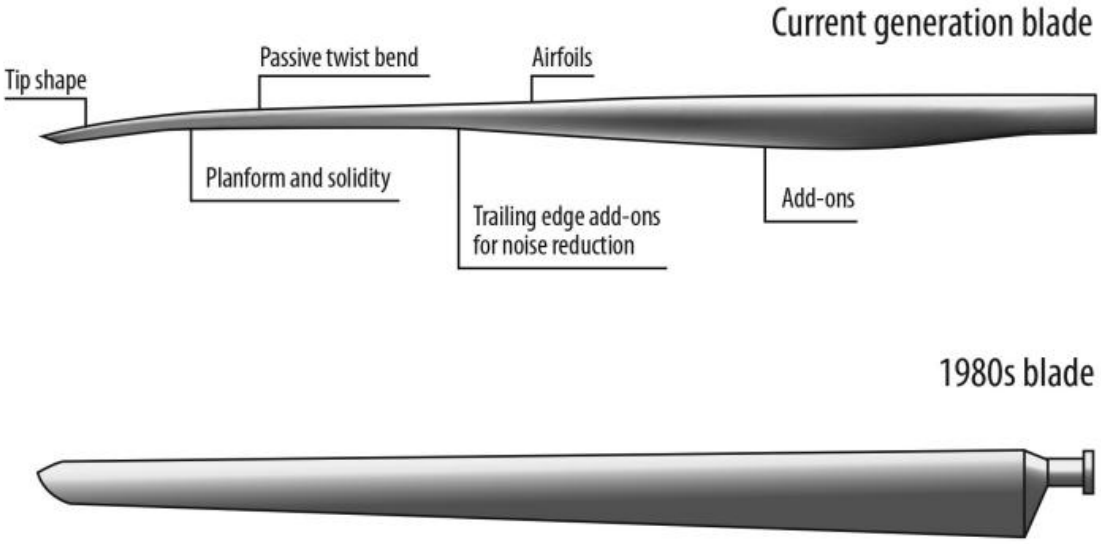

Figure 1.1 Wind turbine blade innovation comparing a modern commercial blade (top) and a commercial *blade from the mid-1980s (bottom) scaled to the same length. The modern blade is 90% lighter than the scaled 1980s technology*

Thus, the insights provided by Veers et al. (2019) offer a valuable framework for guiding the research and development efforts in this thesis. By aligning the development of PTV test protocols with the broader challenges in wind energy research, this work aims to contribute to the advancement of wind energy technology and the realization of its full potential as a major source of clean, renewable energy[13].

Recent research on tidal energy has provided valuable insights into the development of test protocols for Particle Tracking Velocimetry (PTV) in turbine wake analysis. Comparative studies conducted across different experimental facilities have played a crucial role in understanding the performance and behavior of tidal turbines, which are vital for optimizing energy extraction in marine environments[13].

These studies involved testing a three-bladed horizontal-axis turbine model in multiple facilities to ensure consistent evaluation. The facilities included two towing tanks, one at CNR-INSEAN in Rome and another at Strathclyde University in Glasgow, as well as two circulating water channels at CNR-INSEAN and IFREMER in Boulogne-sur-mer. The experiments aimed to compare performance metrics such as torque, drag, and inflow speed to determine how different test environments affect the results. A significant finding from this research was that while the overall performance assessments of the turbine were consistent across the facilities, there were notable differences in the fluctuations of torque and drag. These discrepancies were largely

attributed to blockage effects, which had a significant impact even at low blockage ratios. Blockage effects are particularly influential at high thrust coefficients, affecting the accuracy of torque and drag measurements. Understanding these effects is crucial for developing precise PTV protocols[14].

The studies also highlighted the importance of key parameters such as blockage ratio and turbulence intensity in influencing the behavior of tidal turbines. Towing tanks, due to their varying lengths, provided different acquisition times and flow conditions, which influenced the measurements. In contrast, circulating water channels offered controlled flow environments with adjustable turbulence levels, allowing for a more stable and consistent evaluation of turbine performance.

These comparative analyses emphasize the necessity for standardized testing protocols to ensure reliable and comparable results across different experimental facilities. For researchers focused on developing PTV test protocols for turbine wakes, incorporating these findings is essential to enhance the accuracy and reliability of their experimental outcomes. By accounting for the unique characteristics and influences of different test environments, researchers can create more robust protocols that improve the optimization and performance evaluation of tidal energy devices[14].

Incorporating the insights from these studies into the development of PTV test protocols will significantly contribute to the advancement of tidal energy research. Accurate and reliable PTV methods will provide detailed insights into the wake dynamics and flow interactions of tidal turbines, which are essential for designing efficient turbines that can operate effectively in clustered tidal farm environments. This work aims to ensure that the methods used are both precise and applicable across various testing scenarios, ultimately contributing to the optimization of tidal energy systems and their integration into the broader renewable energy landscape[15].

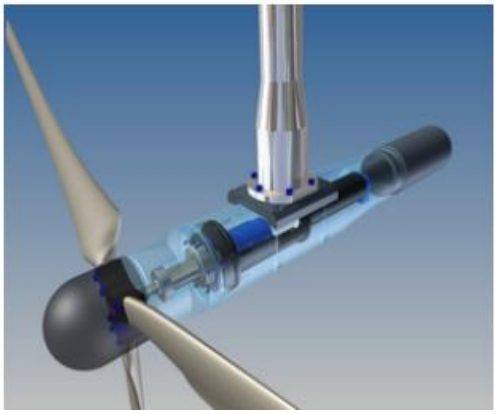

Figure 1. 2: 3D CAD view of the turbine

Figure 1.3: Views of the turbine in the IFREMER flume tank at rest, during a measurement in the KHL towing tank from an underwater camera, in the empty CNR-INSEAN flume tank and during a carriage reverse in the CNR-INSEAN towing tank, from the left to the right.

Model-scale studies have played a crucial role in the design and optimization of offshore wind turbine systems. These studies involve the construction and testing of scaled-down models of wind turbines in controlled environments, such as wind tunnels or wave tanks. By replicating real-world conditions on a smaller scale, researchers can assess the aerodynamic and hydrodynamic performance of wind turbines, optimize their design parameters, and predict their behavior in offshore environments[16].

Model-scale studies offer several advantages in the development of offshore wind turbines. Firstly, they provide a cost-effective means of testing new designs and concepts before full-scale deployment. By conducting experiments on model turbines, researchers can iterate and refine their designs, minimizing the risk of costly errors during the construction and operation of full-scale turbines. Additionally, model scale studies allow researchers to investigate specific phenomena, such as aerodynamic

loads, turbulence effects, and wake interactions, in a controlled and reproducible manner[16].

Several methodologies are commonly employed in model scale studies of offshore wind turbines. Wind tunnel testing is widely used to assess the aerodynamic performance of turbine blades and the interaction between turbines in wind farms. By subjecting scaled-down turbine models to airflow under controlled conditions, researchers can measure parameters such as lift, drag, and power output, providing valuable insights for turbine design optimization. Similarly, wave tank testing allows researchers to study the hydrodynamic behavior of floating wind turbine platforms and their response to wave loading and mooring systems[17].

Numerical modeling techniques, such as computational fluid dynamics (CFD), complement experimental studies by simulating the flow behavior around wind turbines in offshore environments. CFD simulations enable researchers to investigate complex flow phenomena, such as turbulent wakes, boundary layer interactions, and dynamic stall, with high spatial and temporal resolution. By integrating experimental and numerical results, researchers can gain a comprehensive understanding of wind turbine aerodynamics and hydrodynamics, facilitating informed design decisions for offshore wind farms[18].

Several notable studies have demonstrated the value of model scale testing in advancing offshore wind turbine technology. For example, the European project "DeepWind" conducted extensive model scale testing to assess the performance of floating offshore wind turbine concepts in deep waters. Similarly, research conducted at the WindEEE Dome facility in Canada has contributed to the development of innovative wind turbine designs and offshore wind farm layouts through scaled-down experiments in a three-dimensional wind tunnel environment. These studies have shown that model scale testing is an effective approach for improving the performance and reliability of offshore wind turbines[19].

a critical aspect of wake recovery in offshore wind farms is the assessment of the fluid domain surrounding turbines. Understanding the wake recovery fluid domain involves analyzing how the turbulent wake generated by a wind turbine interacts with the surrounding flow field and dissipates over time. This information is essential for optimizing wind farm layout and turbine spacing to minimize wake effects and

maximize energy production. Experimental studies and numerical simulations are used to characterize wake recovery fluid domains, providing insights into the dynamics of wake decay and its impact on downstream turbines[19].

In offshore wind farms, the wake recovery fluid domain plays a crucial role in determining the efficiency and performance of the entire wind farm. As wind turbines extract energy from the oncoming wind, they create turbulent wakes downstream, characterized by reduced wind speeds and increased turbulence intensity. Understanding how these wakes evolve and dissipate as they propagate through the wind farm is essential for optimizing turbine placement and maximizing energy yield[20].

Experimental studies involving instruments such as LIDAR (Light Detection and Ranging) and Doppler anemometers are commonly used to measure wind speed and turbulence characteristics within wake recovery fluid domains. These measurements provide valuable data for validating numerical models and assessing the accuracy of wake prediction tools. For instance, studies conducted by Larsen and Hansen (2017) have utilized LIDAR technology to investigate wake recovery characteristics in offshore wind farms, highlighting the importance of wake dynamics in wind farm performance optimization[20].

Numerical simulations, based on computational fluid dynamics (CFD) models, complement experimental studies by offering insights into the underlying physics of wake recovery and its interaction with complex environmental factors such as atmospheric stability and wind shear. Research conducted by Barthelmie and Pryor (2014) has employed CFD simulations to analyze meteorological controls on wind turbine wakes, emphasizing the role of atmospheric conditions in wake evolution and recovery.

By analyzing wake recovery fluid domains, researchers can develop strategies to mitigate wake effects and improve overall wind farm performance. For example, optimizing turbine spacing and layout based on wake recovery characteristics can minimize energy losses due to wake interactions, resulting in higher energy production and increased revenue for wind farm operators[21].

The assessment of the fluid domain surrounding offshore wind turbines is a critical aspect of wake recovery in wind farms. In order to optimize wind farm layout and turbine spacing to minimize wake effects and to maximize energy production, it is

essential to understand how the turbulent wake generated by a wind turbine interacts with the surrounding flow field and dissipates over time. Experimental studies and numerical simulations are used to characterize the wake recovery fluid domains, providing valuable insights into the underlying physics of wake recovery and its interaction with complex environmental factors such as atmospheric stability and wind shear[22].

In offshore wind farms, the wake recovery fluid domain plays a crucial role in determining the efficiency and performance of the entire wind farm. As wind turbines extract energy from the oncoming wind, they create turbulent wakes downstream, characterized by reduced wind speeds and increased turbulence intensity. Understanding how these wakes evolve and dissipate as they propagate through the wind farm is crucial for optimizing turbine placement and maximizing energy yield.

Experimental studies involving advanced instruments such as LIDAR (Light Detection and Ranging) and Doppler anemometers are commonly used to measure wind speed and turbulence characteristics within wake recovery fluid domains. These measurements provide valuable data for validating numerical models and assessing the accuracy of wake prediction tools. For instance, studies conducted by Larsen and Hansen (2017) have utilized LIDAR technology to investigate wake recovery characteristics in offshore wind farms, highlighting the importance of wake dynamics in wind farm performance optimization.[22]

Numerical simulations, based on computational fluid dynamics (CFD) models, complement experimental studies by offering insights into the underlying physics of wake recovery and its interaction with complex environmental factors such as atmospheric stability and wind shear. Numerical simulations provide a powerful tool for optimizing turbine layout and spacing and assessing the impact of wake interactions on energy production.

By analyzing wake recovery fluid domains, researchers can develop strategies to mitigate wake effects and improve overall wind farm performance. For example, optimizing turbine spacing and layout based on wake recovery characteristics can minimize energy losses due to wake interactions, resulting in higher energy production and increased revenue for wind farm operators. Therefore, understanding the

dynamics of wake decay and its impact on downstream turbines is essential for the efficient design and operation of offshore wind farms[23].

Although testing at a smaller scale may have its limitations, laboratory testing remains a vital aspect of device design. It offers valuable insights into device behavior in controlled environments, which informs numerical modeling methods and their associated design coefficients. Fine-tuning and validation against measurements from a controlled laboratory environment is key. Whether designing wind turbines or tidal stream turbines, water tank testing has provided valuable data on rotor loading, device wake recovery, and farm/array interactions.

Before utilizing new experimental equipment, it is crucial to evaluate its accuracy and determine any potential sources of uncertainty in the resulting data. As each facility may have distinct testing procedures, standardizing the methodologies employed becomes necessary. To assess the impact of the hydrodynamic testing facility on the performance of modelscale tidal turbines, the authors conducted identical measurements using a standard protocol at three separate facilities: CNRINSEAN, IFREMER, and the Kelvin Hydrodynamics Laboratory (KHL).

The researchers noted variations in thrust and power over time, which they attributed to dissimilarities in turbulence inflow between recirculating flumes and towing tanks affected by carriage vibrations. In addition, they carried out 'Blind test' assessments to evaluate the aerodynamic performance and wakes of wind turbines. These datasets have proven to be highly valuable in facilitating industry comparisons of numerical modeling.

2.1. Background and geometry

MarinLab, a state-of-the-art hydrodynamic research facility, was established in 2016 and is situated at HVL campus in Bergen. As depicted in Figure 1, the facility boasts a 50-meter long tank with a 2.2x3 meter cross-section. Equipped with an Edinburgh Designs towing carriage and six force-feedback flap-type wave paddles, the tank serves as an ideal platform for model scale testing of a range of marine systems including ships, offshore structures, floating platforms, mooring systems, marine energy devices, underwater and autonomous vehicles, and hydrodynamic interactions. MarinLab is committed to supporting the research community.

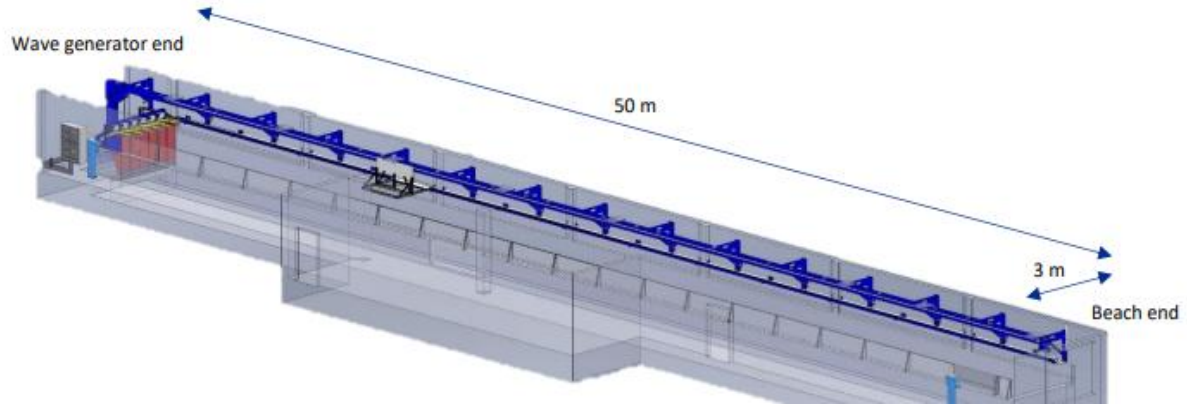

Figure 2.1. showcases six hinged wave paddles that are capable of generating waves with a maximum height of 0.5m at wave periods around 2 seconds.

Regarding Figure 2.1, For wave periods above 0.8 seconds, Figure 4 illustrates that directional spreading of ±90° is achievable. These paddles have force-feedback control, enabling the damping of unwanted tank wall reflections. Figure 3 provides a comprehensive overview of the variety of regular wave conditions that can be created. Additionally, by utilizing JONSWAP, Bretschneider, Pierson-Moskowitz spectra, irregular waves can also be produced. Wave focussing can create design breaking waves, with a repeat period of roughly 20 seconds. Wave synthesis software allows for the generation of many wave types, so please don't hesitate to contact us if you have any unique requirements for your studies.

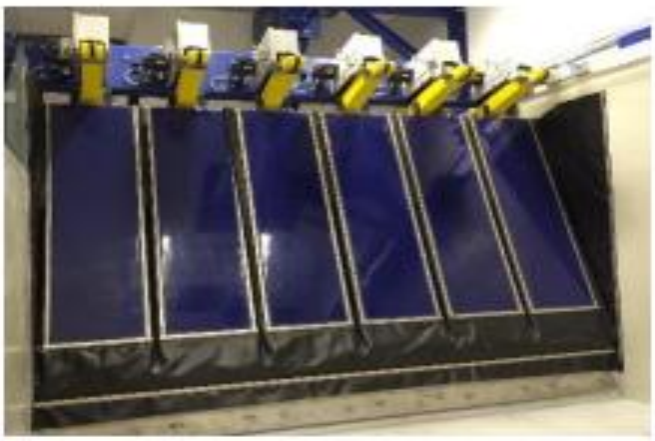

Figure 2.2: Wavemaker with 0.5m wide flaps

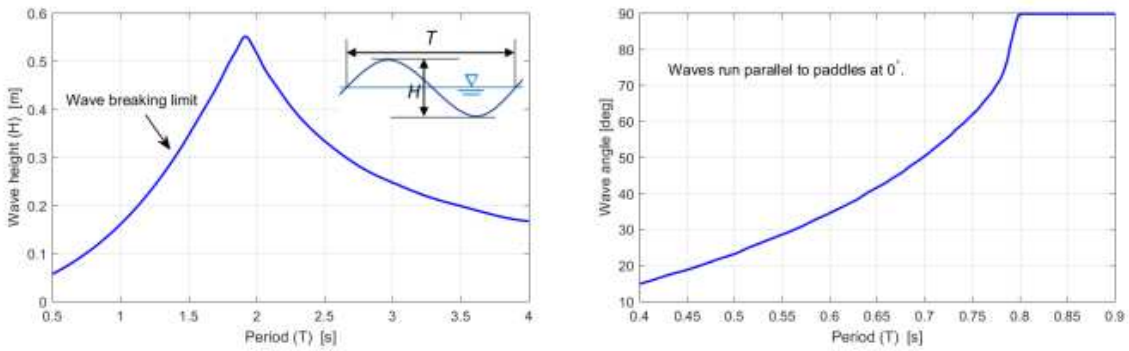

Figure 2.3 (Left) and Figure 2.4 Figure 2.4 (Right): Regular wave generation limits, hinge depth 1.2m, and Wave angle limit of long-crested waves.

In contrast to the wave paddles, a porous passive beach is installed in the tank as shown in Figure 5. The beach is designed with an exponential profile to effectively absorb breaking waves and minimize reflections. Its angle asymptotes to 8°, making it an ideal setting for studying wave breaking caused by depth changes.

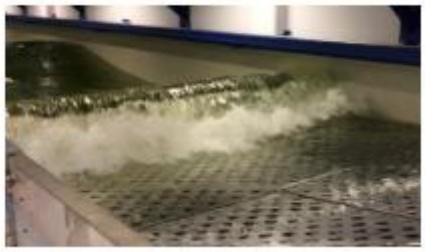

Figure 2.5: Wave absorbing porous beach

This tank is equipped with two towing carriages that can tow at a maximum velocity of 5.0 m/s and an acceleration of 1.2 m/s2, with a precision of 0.001 m in positioning. To minimize blockage effects (< 5%), the test-bed dynamometer is optimized for rotor diameters, D = 2R, typically ranging from 0.5-0.6 m, and a maximum tip-speed ratio, T SR (Eq.(1)), of around 10 at an inflow velocity of U∞ = 1 m/s. These specifications determine the design parameters for the turbine drive-train, with projected maximum thrust and torque in the vicinity of 120 N and 4 Nm, respectively. T SR = ωR U∞ (1) In Equation (1), ω represents the rotor's rotational speed in rad/s.

In their study, the turbine was 1.2 m diameter and bed-supported, with transducers measuring thrust and torque on the rotor and streamwise root bending moment on each blade. However, due to the smaller rotor diameter and hence smaller torque

requirements in the MarinLab, a narrower nacelle and corresponding motor/gearbox diameter has been incorporated.

A torque-thrust (QT) transducer of 5 Nm and 100 N capacities, with similar design to [24] has been custom made by Marin, Netherlands. A 480 W Mean Well 48V DC power supply (HEP-480-48A) is used for powering the dynamometer, with any excess power generated being absorbed by a 50 Ω resistor with 200 W rating (RS200). After two design iterations of the aluminum nacelle housing, the final outer diameter around the central tower-nacelle connection boss is 96 mm, with an overall length of 760 mm. Prior to assembly with the dynamometer electronics, a water-tightness test conducted under a compressed air supply, found a leak at the top of the tower-nacelle boss and required a new O-ring groove to be machined. A humidity sensor (DHT11) was subsequently added at the tower nacelle interface, connected to LabView via an Ardunio microprocessor to provide a warning alarm should the humidity level exceed 60%, indicating possible water ingress. A. Rotor design In order to benchmark the test-bed, the well documented rotor geometry from [11], [14], [22] with diameter, D = 0.7 m and NACA 633-418 airfoil section is chosen, despite being larger than the diameter range of the design envelope. In order to not exceed the torque capacity from the QT-sensor, the inflow speed is limited to max{U∞} = 0.8 m/s. The foil coordinates from [25] are shown in Figure 1 and the chord and twist distribution is identical to those given in [11]. The available print volume is limited to 220 × 200 × 250 mm whilst the total blade length is 296 mm, so the inner third of the blade (root) is printed separately to the outer two-thirds of the blade (tip). The two sections are joined with universal water-resistant glue and two M5 threaded rods, to prevent excessive torsion and bending of the blade tip. The minimum trailing edge thickness was defined to 0.2 mm. The three blades took approximately 36 hours to print and were lightly handsanded with 600 g/m2 paper to remove minor surface defects at the leading edge.

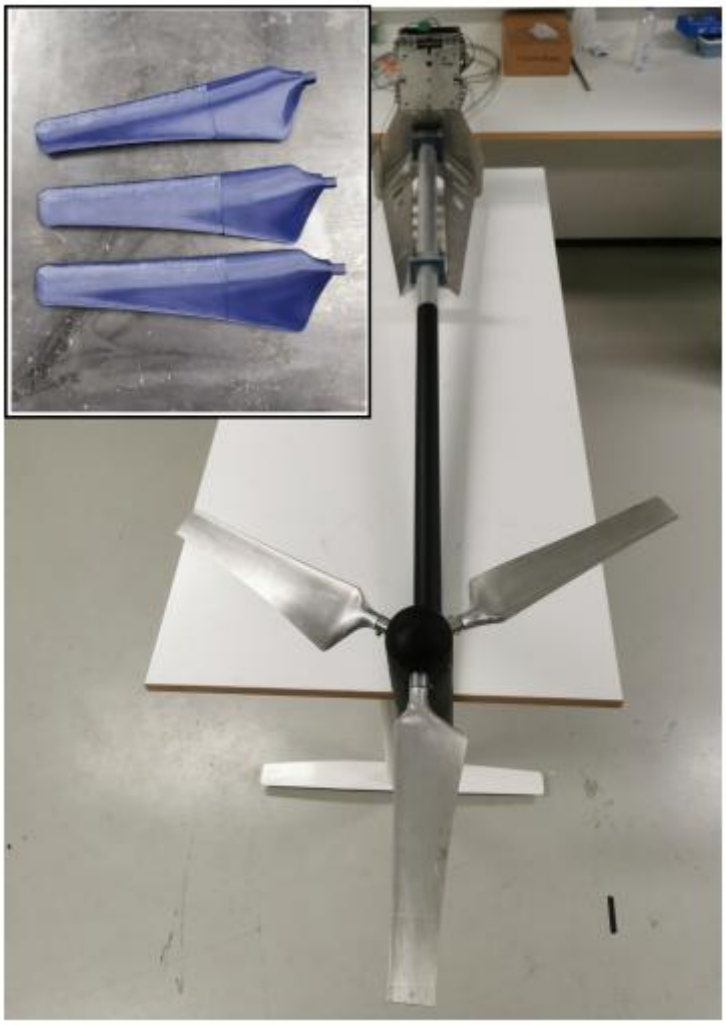

Figure 2.6: Turbine blades in 2 different materials

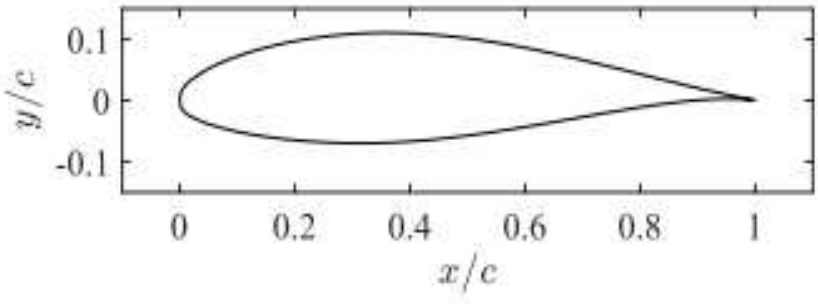

Figure 2.7: The turbine blade airfoil

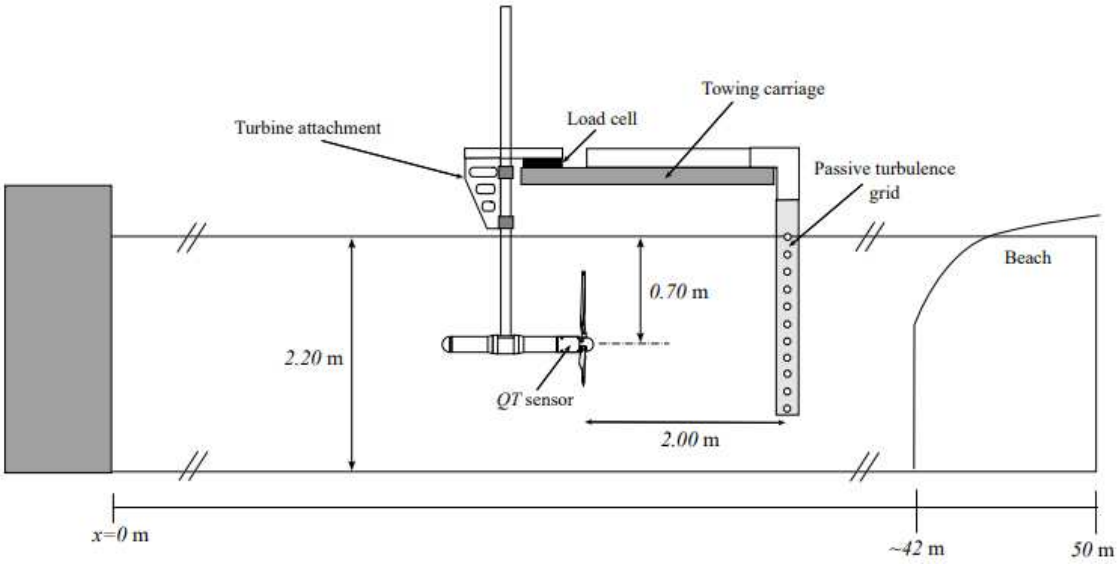

Figure 2.8: The turbine (with all equipment) and its carriage dimensions

Recent studies conducted by Skoland [19] and Koi [20] have utilized an Acoustic Doppler Velocimetry (ADV) approach to measure velocity in the wake of a single point. This method is time-consuming and requires multiple measurements to generate a single wake profile. However, a newly acquired Particle Image Velocimetry (PIV) system could offer more advantages as it can detect and map flow effects more extensively. With the camera system, more information about velocity deficits upstream and downstream of different multirotor configurations can be obtained. Additionally, vortex formation can be investigated by imaging a specific subvolume of the flow, which is impossible with an ADV.

The main aim of this thesis is to establish a PIV measurement methodology for use in a towing tank, characterize the near wake of a horizontal axis turbine.

2.2.Background Theory

Actuator Disk Theory

The actuator disk theory is a fundamental model used to understand the aerodynamics of wind and tidal turbines. It conceptualizes the turbine as a permeable disk that exerts a uniform force on the fluid passing through it, enabling the calculation of critical performance parameters such as thrust and power coefficients.

Basic Principles of Actuator Disk Theory

The actuator disk theory relies on the principles of conservation of mass, momentum, and energy. As fluid flows through the disk, it experiences a pressure drop, leading to a reduction in velocity. The fundamental steps include:

Conservation of Mass: The mass flow rate remains constant through the disk:

$$\dot{m} = \rho A V1 = \rho A V2 \quad \{4.1\}$$

where $\dot{m}$ is the mass flow rate, ρ is the fluid density, A is the disk area, $V1$ is the velocity upstream, and $V2$ is the velocity at the disk.

Conservation of Momentum

The thrust T produced by the disk is equal to the change in momentum of the fluid:

$$T = \dot{m}(V1 - V2) \quad \{4.2\}$$

Bernoulli's Equation: This relates the pressure and velocity changes across the disk:

$$P1 + 1/2\rho V_1^2 = P2 + 1/2\rho V_2^2 \quad \{4.3\}$$

where $P1$ and $P2$ are the pressures upstream and downstream, respectively.

2.3. Key Concepts and Equations

Induction Factor (a): This factor represents the fraction of velocity reduction at the disk:

$$V2 = V1(1 - a) \quad \{4.4\}$$

Power Coefficient (Cp): Defined as the ratio of the power extracted by the turbine to the power available in the undisturbed flow:

$$Cp = 4a(1 - a)2 \quad \{4.5\}$$

Thrust Coefficient (Ct): Defined as the ratio of the thrust force to the dynamic pressure force:

$$Ct = 4a(1 - a) \quad \{4.6\}$$

Experimental Validation

Extensive experiments have validated the actuator disk theory, revealing critical insights:

Velocity Distribution: Velocity deficits follow a Gaussian distribution in the far wake if not constrained by tank walls.

Thrust Coefficients: Larger disks show higher thrust coefficients due to increased blockage effects.

Axial Induction Factor: Thrust and power coefficients vary with the axial induction factor, which is critical for understanding turbine performance.

Blockage Corrections: Blockage corrections significantly influence the measured coefficients, highlighting the importance of considering tank dimensions.

Standardized Testing Protocols: Consistent testing protocols across different facilities ensure reliable results, emphasizing the need for standardized methodologies.

Discrepancies in Measurements: Differences in experimental setups can lead to discrepancies in torque and drag measurements, underscoring the importance of harmonized testing conditions.

To support the theoretical explanations, the following figures are essential:

1. Effects of Fluid Passing Through an Actuator Disk: Illustrates velocity deficit and pressure drop.

2. Variation of Power and Thrust Coefficients with Axial Induction Factor: Highlights theoretical limits and practical applications.

3. Translated Diagrams on Thrust and Power Coefficients: Demonstrates the impact of blockage corrections.

4. Standardized Testing Protocols: Shows the importance of consistent methodologies across different experimental setups.

These insights collectively underscore the relevance of actuator disk theory in the design and analysis of turbine wakes, providing a robust foundation for developing test protocols for Particle Tracking Velocimetry (PTV) in towing tanks. Integrating these theoretical foundations and experimental validations will offer a comprehensive understanding of the actuator disk theory's application in tidal turbine wake studies. This approach will enhance the reliability of PTV techniques and contribute to the optimization of tidal energy systems.

2.4. Blade Element Momentum (BEM) Theory

Overview

The Blade Element Momentum (BEM) theory combines two methods, the blade element theory and momentum theory, to analyze the performance of turbine blades. This theory is widely used for the design and analysis of wind and tidal turbines due to its balance of simplicity and accuracy.

2.4.1. Principles of BEM Theory

Momentum Theory:

Axial and Angular Momentum: The theory applies conservation of linear and angular momentum to an annular control volume around the rotor.

Thrust and Power: It calculates the thrust and power generated by the turbine by considering the change in momentum of the fluid passing through the rotor disk.

Blade Element Theory:

- **Airfoil Characteristics**: The rotor blade is divided into small elements, and the forces on each element are determined based on the local flow conditions and airfoil characteristics. Lift and Drag: Each blade element contributes to the overall lift and drag forces, which are integrated to find the total thrust and torque on the rotor.
- **Mathematical Formulation:** Axial Induction Factor (a) describes the fractional decrease in wind speed at the rotor disk:

$$\boldsymbol{Vd = V\infty(1 - a)} \quad \textbf{\{4.7\}}$$

1. where Vd is the velocity at the disk and $V\infty$ is the free stream velocity.
2. Tangential Induction Factor (a'): Describes the effect of rotation on the flow

$$\boldsymbol{\omega d = \omega\infty(1 + a')} \quad \textbf{\{4.8\}}$$

1. where ωd is the angular velocity at the disk and $\omega\infty$ is the free stream angular velocity.

Blade Element Forces:

1. Normal Force (dF_n): Perpendicular to the rotor plane:

$$\boldsymbol{dFn = 21\rho V2(clcos\phi + cdsin\phi)cdr} \quad \textbf{\{4.9\}}$$

2. Tangential Force (dF_t): Parallel to the rotor plane:

$$\boldsymbol{dFt = 12\rho V2(clsin\ \phi - cdcos\ \phi)cdrdFt = 21\rho V2(clsin\phi - cdcos\phi)cdr} \quad \textbf{\{4.10\}}$$

3. where ρ is the fluid density, V is the relative velocity, cl and cd are the lift and drag coefficients, ϕ is the flow angle, c is the chord length, and dr is the radial element width.

Thrust and Torque:

a. **Thrust (T):** Summed over all blade elements:

$$\mathbf{T = \int 0RdFndrT = \int 0RdFndr} \quad \textbf{\{4.11\}}$$

b. **Torque (Q):** Resulting from tangential forces:

$$\boldsymbol{Q = \int 0RrdFtdrQ = \int 0RrdFtdr} \quad \textbf{\{4.12\}}$$

2.4.2. Corrections and Extensions

Tip Loss Correction (Prandtl's Tip Loss Factor): Accounts for the finite number of blades and their tip vortices, reducing the effective inflow:

$$\mathbf{F = 2\pi cos\ -1(exp\ (-B(R-r)2rsin\ \phi))F = \pi 2cos - 1(exp(-2rsin\phi B(R-r)))}$$
{4.12}

where B is the number of blades, R is the rotor radius, and r is the local radius.

Glauert Correction: Adjusts the axial induction factor in high-thrust conditions to account for non-linear effects.

The BEM theory is validated through various experimental setups, including towing tanks and wind tunnels.

2.4.3.Reynolds Number

The Reynolds number (Re) is a dimensionless quantity used to predict flow patterns in different fluid flow situations. It is defined as the ratio of inertial forces to viscous forces within a fluid flow and is a key parameter in characterizing the nature of the flow around turbine blades and in their wakes.

Mathematical Definition:

$$Re = \frac{\rho UL}{\mu} = \frac{UL}{\nu} \quad \textbf{\{4.12\}}$$

where:

- ρ is the fluid density
- U is the characteristic velocity
- L is the characteristic length (such as the chord length of the blade)

- μ is the dynamic viscosity
- ν is the kinematic viscosity

2.5 Characteristics of Turbulent Wake

Velocity Deficit:

The reduction in flow velocity behind the turbine is due to the extraction of kinetic energy. This deficit recovers as the flow moves downstream, influenced by turbulence and mixing.

Turbulence Intensity:

The wake region is characterized by high turbulence intensity, which affects downstream turbines in an array. Turbulence intensity influences the mixing rate and wake recovery distance.

Wake Structure:

The near wake region is dominated by coherent vortices shed from the blade tips and trailing edges. The far wake region transitions to a more isotropic turbulent flow.

3. Methodology

The following section outlines the methodology employed for the installation and operation of the Particle Image Velocimetry (PIV) system for this study.

Wave Maker and Wave Dynamics

In the experiment setup, a wave maker was utilized to create various types of waves to achieve an even distribution of particles in the water. It is essential to comprehend the characteristics of these waves to study the flow dynamics around the turbine.

Shallow and Deep Waves

- Shallow Waves**:**

  Shallow waves occur in water where the depth is less than half the wavelength of the wave. These waves have significant horizontal motion, which causes particles and water to move predominantly in the horizontal plane. The horizontal motion of shallow waves helps to mix particles laterally, ensuring an even distribution across the width of the tank.
- Deep Waves:

  Deep waves, on the other hand, form in water where the depth is greater than half the wavelength of the wave. These waves are characterized by their vertical motion, which moves particles and water up and down. The vertical motion of deep waves contributes to the vertical mixing of particles, helping to achieve a uniform particle distribution throughout the entire depth of the tank.

By operating the wave maker at different frequencies, both shallow and deep waves were generated. This combination of wave types ensured thorough mixing of the particles, creating a homogeneous particle distribution in the water, which is essential for accurate flow measurement and analysis.

3.1. Lagrangian Flow

The concept of Lagrangian flow involves studying fluid motion by carefully tracking the movement of individual particles as they travel through the fluid. This thesis focuses on the use of a Lagrangian Particle Tracking Velocimetry (LPTV) system to capture and analyze how particles move in relation to a stationary turbine and camera setup. When the turbine operates at a towing speed of 0.8 m/s, the particles are suspended

in the water and illuminated by a consistent light source. It's important to note that although the particles themselves remain stationary in the tank, they appear to move relative to the turbine and camera system. This setup allows for detailed recording of particle trajectories, offering valuable insights into the dynamics and interactions within the fluid environment.

3.2. Installation of the PIV System

Setup Overview:

To capture the detailed flow characteristics around the turbine, a PIV system was installed. This included setting up lighting, positioning the turbine on the carriage, and arranging the camera system.

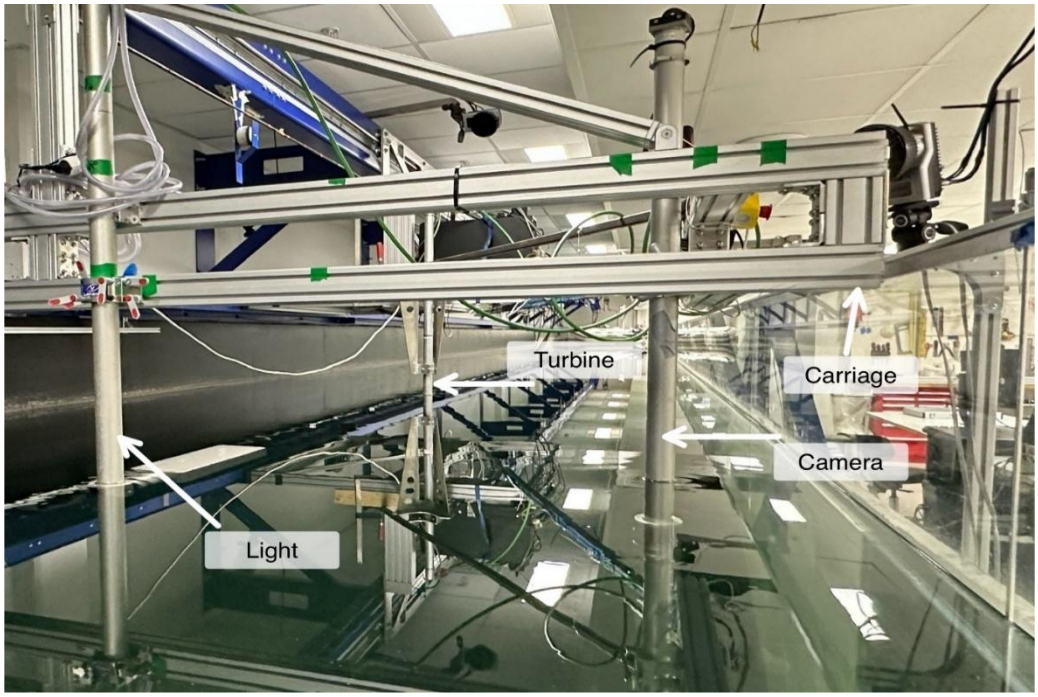

Figure 3.1: Position of the Turbine and related equipment

Figure 3.2: Lightning system and camera

Lighting Installation:

The lighting system was installed on the carriage alongside the turbine. This ensured consistent illumination of the flow field, which is critical for capturing high-quality images of the particles in the water.

Figure 3.3: Lightning system from a closer view, in 45-degree mode(turning the elbow from 90 degrees to 45 degrees to have the lights from the upside of the turbine)

Figure 3.4: Lightning system and camera, disassembled from the PC

Turbine Setup:

The turbine was mounted securely on the carriage. The carriage moved along a 30-meter section of the towing tank at a fixed speed of 0.8 m/s.This setup provided a controlled environment to simulate real-world operating conditions for the turbine.

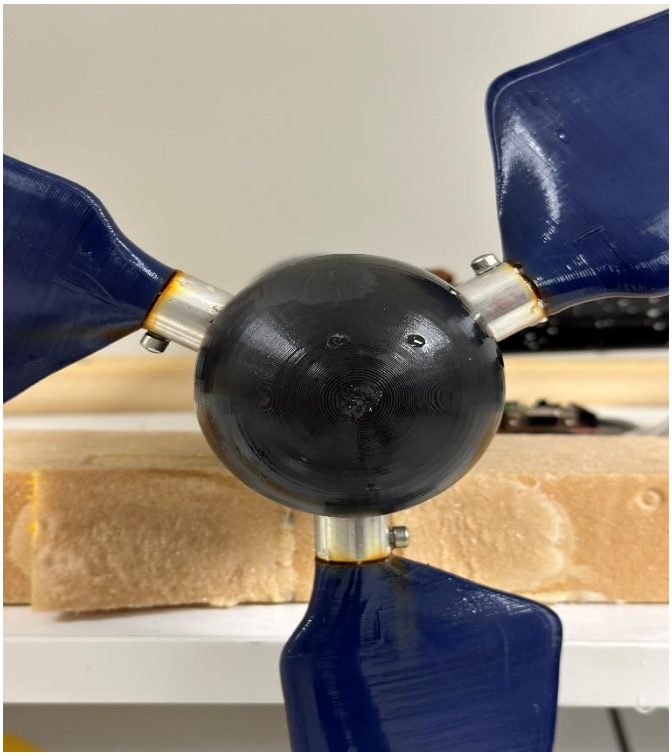

Figure 3.5 The Turbine blades and its nassale from a close view

Camera Arrangement:

The camera system was installed to capture images from the side of the turbine.

Four lenses were arranged in a row to cover the necessary field of view and ensure sufficient spatial resolution.

Figure 3.6: Camera of the PIV system

Calibration:

Before running the turbine, calibration of the camera system was performed using a dotted calibration board. This step was crucial to ensure accurate positional data of

the particles, which were injected into the flow field. Each particle used in the experiment had a diameter of 1 micron. The calibration process involved:

Positioning the Calibration Board:

The dotted calibration board was placed in the camera's field of view. Calibration images were captured to map the camera's pixel coordinates to real-world coordinates.

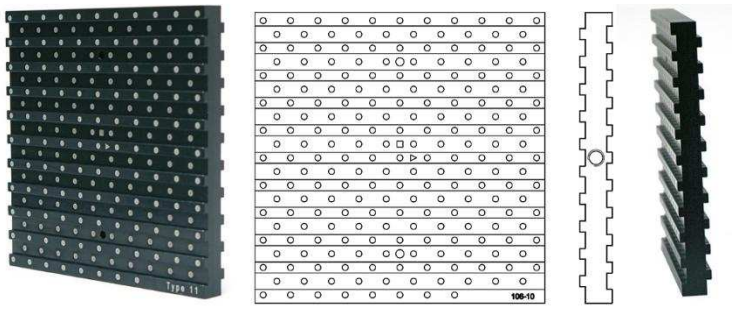

Figure 3.7: Calibration Plate of the PIV system

Calibration Verification:

The captured calibration images were processed to verify the accuracy of the camera setup.This ensured that after particle injection, the system could accurately track the position of each particle.A grid of the ideal regular grid of marks is overlayed in green. This grid should pass through the center of all marks.

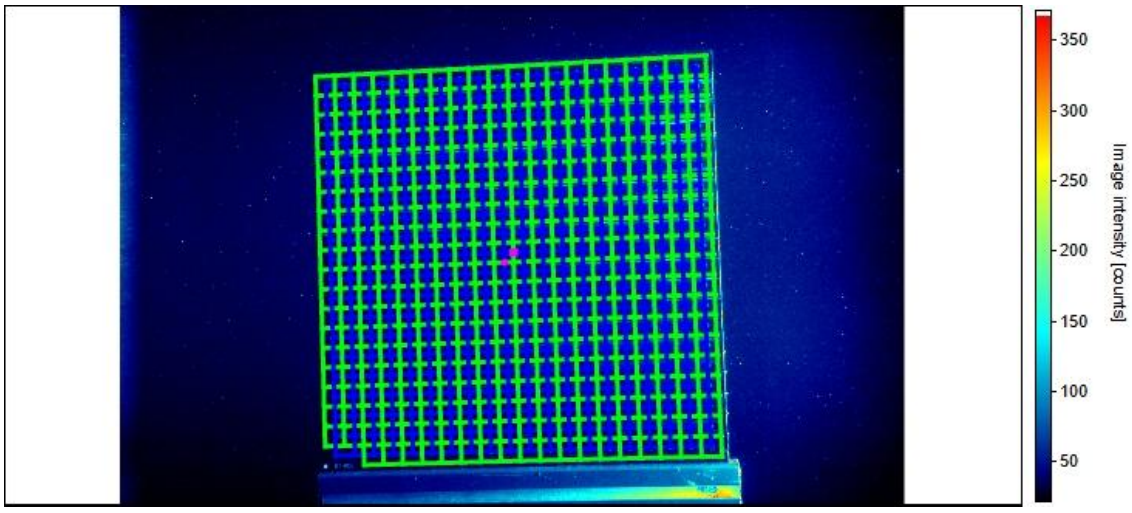

Figure 3.8: Recorded image of the Calibration Plate of PIV system from the camera view

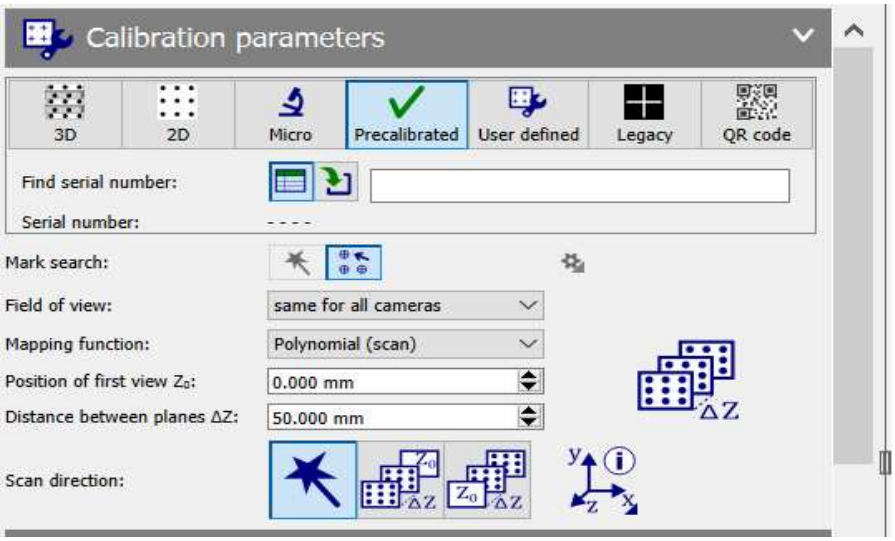

Figure 3.9: Calibration Mode of the Davis Software

Selecting the used type of plate from the Calibration plate list in the corresponding sections 3D, 2D, Micro, Precalibrated, User defined, Legacy.

Precalibrated: Calibration plate with measured mark positions of all dots. Either enter a serial number of the calibration plate or select the MCP file provided by LaVision.

Depending on the calibration plate, we can decide between automatic or manual mark search. The automatic mark search should work in most cases.

Depending on our physical setup, we can select the appropriate Mapping function. (see section Limitations and Requirements for Pinhole / Polynomial Mapping Function).

-In case of a polynomial scan, define the distance between each calibration view.

-In case of a polynomial scan, define the scan direction. The automatic mode should determine the direction correctly in most (not microscopic) cases.

Perspective Calibration is Necessary If the camera is not looking perpendicular to the measurement plane or if lens distortions are present (typically radial barrel and cushion distortion), the image distortions need to be corrected. Otherwise, it is not possible to define axis orientations and a pixel/mm scaling that is valid for the entire image. In order to calculate further derivatives (e.g., a PIV calculation), an image correction is required as an intermediate step.

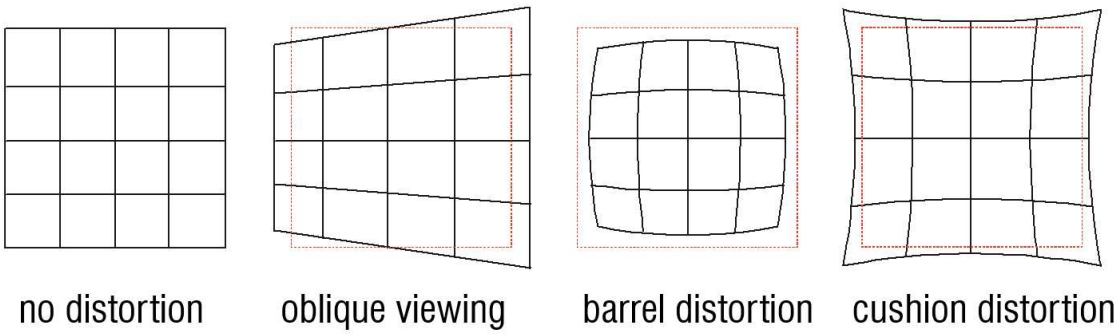

Figure 3.10: Different types of detected plate

3.3. Experimental Procedure

Running the Turbine:

Flow Initialization: The carriage, along with the turbine and lighting system, was moved along the 30-meter distance in the towing tank. The turbine was operated at a fixed speed of 0.8 m/s to maintain consistent flow conditions.

Image Capture**:** During the run, images of the flow field were captured using the side-mounted cameras. The high-resolution images enabled detailed tracking of particle movements, allowing for the analysis of wake characteristics behind the turbine.

Live processing section: It allows to monitor the usability of desired processing operations that will be applied to the current Live View. Via the Configure

View Layout button, processing results can be displayed beside the raw camera images. This view is depicted in the figure below.

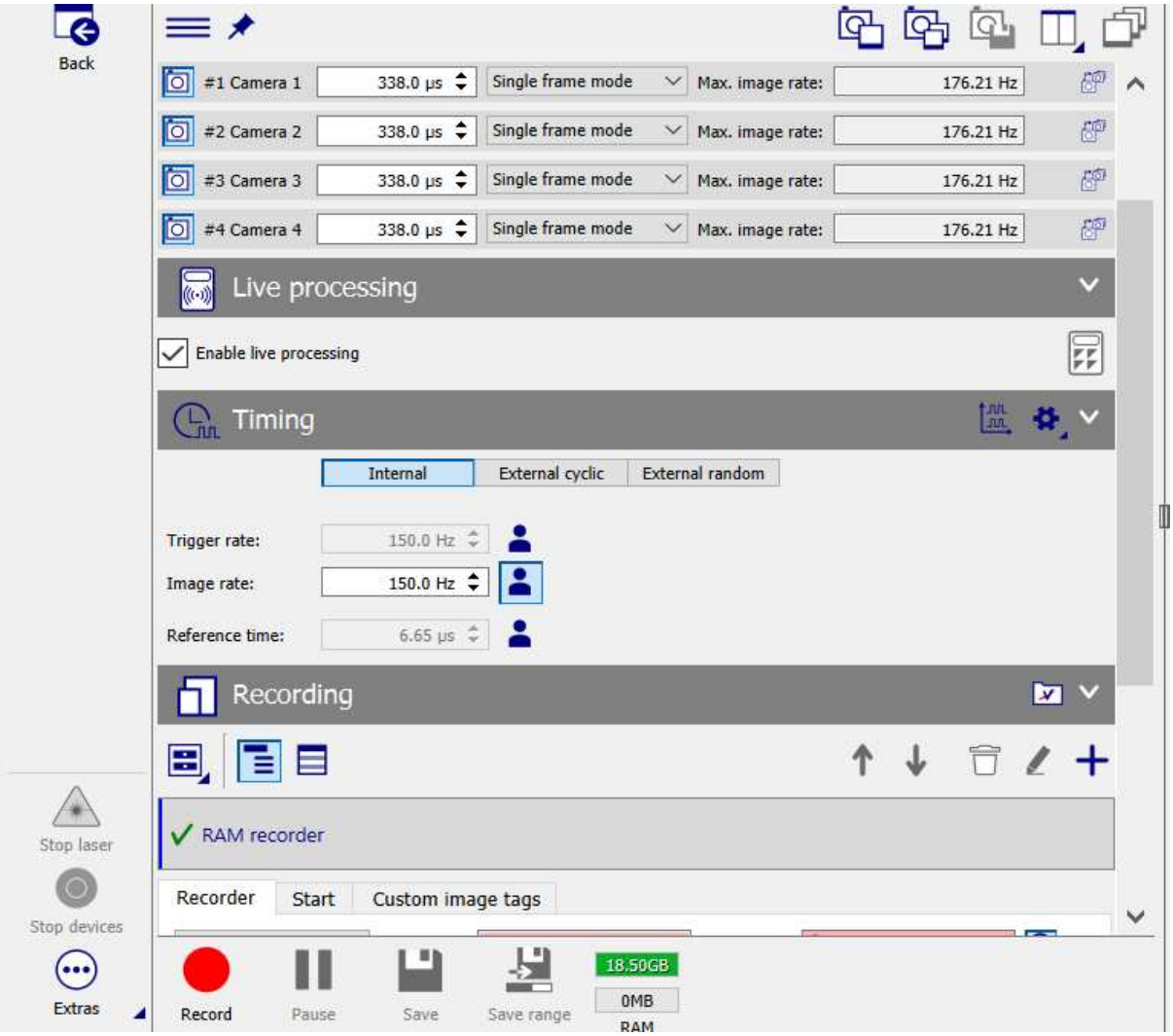

Figure 3.11: Image recording tab

Live processing can be enabled by checking the checkbox Enable live processing. Clicking the Processing button opens the Processing dialog. For this step, it is necessary to have a previously grabbed image or a running live grabber, otherwise, the processing dialog cannot be entered. Here, various operations can be applied. Live processing is only executed during grabbing, i.e. results are not stored. During recording, the live processing is not executed. In case the operation list is invalid or does not contain any processing operations,live processing cannot be performed. Other errors that occur are displayed in info messages. The live frame rate depends on how many operations are utilized.

Timing section: Bundles all settings related to triggering, image rates, and reference times. This section provides a brief description of the timing settings.

Trigger source: determines the origin of the PTU trigger and its general behavior.

• **Internal**: The PTU internal clock generates the trigger signal. This trigger signal has a precise constant frequency. This is the default trigger source for the free running of the system.

• **External** cyclic: A TTL trigger signal needs to be sent to the PTU. It is assumed that this signal is periodic and has a frequency that stays constant during a measurement.

• **External random**: A TTL trigger signal needs to be sent to the PTU. The trigger has no frequency and could even be a single trigger.

Trigger rate settings: The settings for the trigger rate depend on the trigger source settings above. Details are described in the PTU-X manual.

Reference time: The delay of the reference time is set concerning the trigger. In case a reference time has double events (like for PIV), the time between these events, the "dt", can be set here. The number of reference times and if they are double events is set in the details of the PTU hardware settings. Depending on the measurement domain of the PTU, the Reference time can also be set in phase angle degrees instead of time.

Timing diagram: Clicking on this button opens the timing diagram. The timing diagram shows the electric TTL signals and the active times of the devices.

Note: The timing diagram reflects the actual state of all recording settings. E.g.: Laser pulses will only be shown if the laser is activated (’On’ mode).

Device Offset: Clicking on the Details button allows to fine-tune the trigger timing of each device (the time offset to add to the automatically calculated trigger time).

Recording section: In the Recording section (see Fig. 10.16), all settings regarding the recording of image sequences are specified. A simple recording is performed by just typing in the number of images to be recorded and clicking the Record button. Alternatively, a very complex automated scan of, e.g. a reference time combined with an X and Y axis could be parameterized all within this section.

A scan could either be configured as a hierarchical or as a table scan. The hierarchical scan is composed of different scan values and loops nested on different levels, usually used to scan through continuous parameter fields.

A table scan consists of a list of scan points, where each column describes a specific scan value. This type of scan is intended for large, sparse parameter fields.

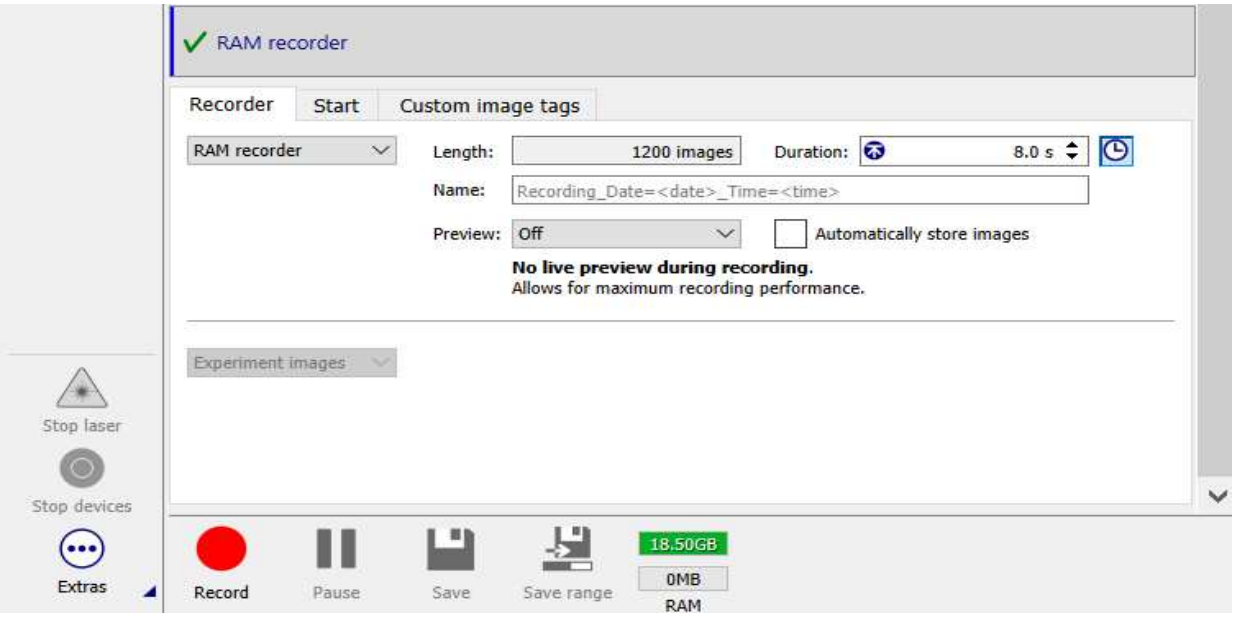

Figure 3.12: Image reccording,starage tab

Resolution of the camera: Camera pixel size in µm. Used in the calibration to get correct pinhole parameters. If this value is set to a wrong value, all pinhole parameters that are scaled in mm, such as focal length or camera–plate distances, will be wrong by the same factor. This will not affect the quality of the calibration! Here is the details of the recorded images:

Component	Technical specifications	
MiniShaker multi-camera	Camera resolution image acquisition Max frame rate Recording rate Camera exposure time Focal length of lenses	896x656 pixels8- or 10-bit 510 fps 150 Hz 200 µs 7.8 mm
LED Flashlight 300	Array areaLEDs Working distance	300 x 100 mm 72 eye-safe high powered500-2000 mm

Table 3.1: Camera and image specification

3.4. Particle Injection and Turbulence Generation

Particle Injection: After calibration and initial image recording, the next step was to introduce particles into the tank.

First Particle Injection: 150 grams of particles were mixed into a 10-liter bucket filled with water. This mixture was then poured into the towing tank. Images were recorded continuously from the moment the particles were added to monitor their distribution.

Figure 3.13: Bucket of particles at the moment of entry

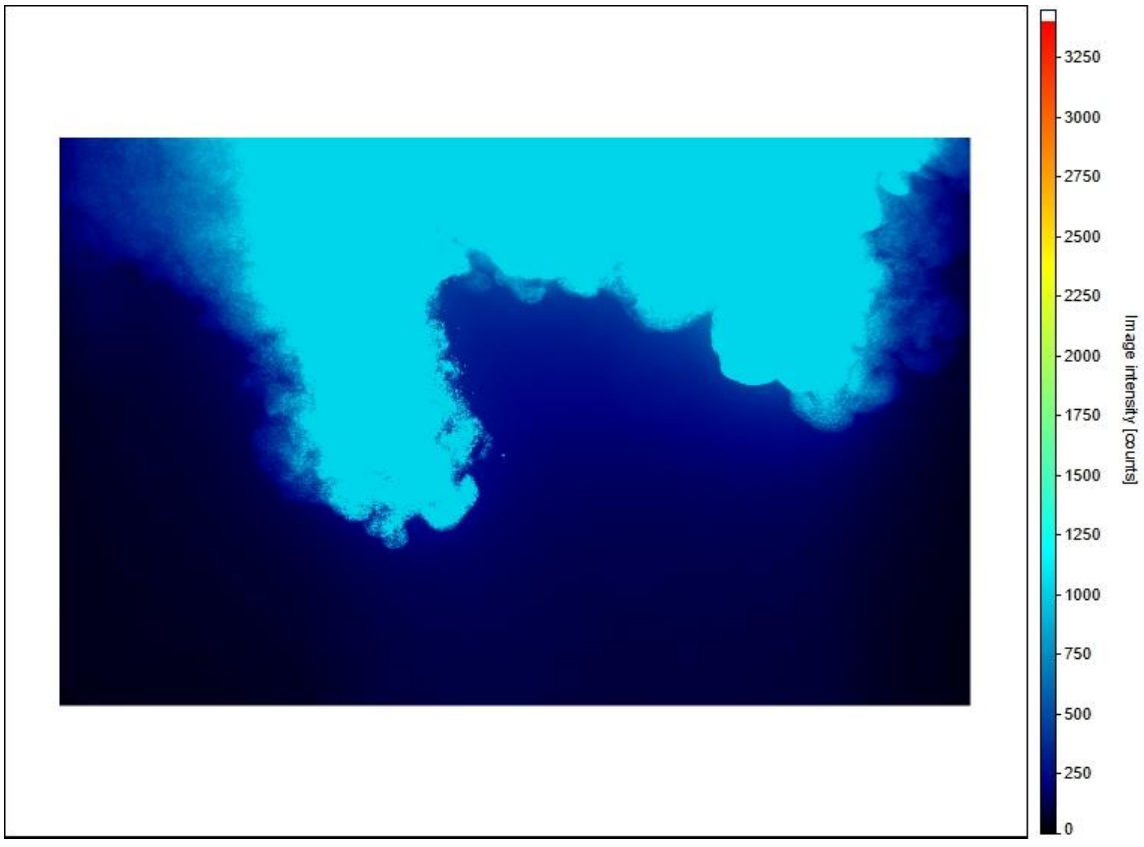

Figure 3.14: Cloud of particles 3 minutes after entry

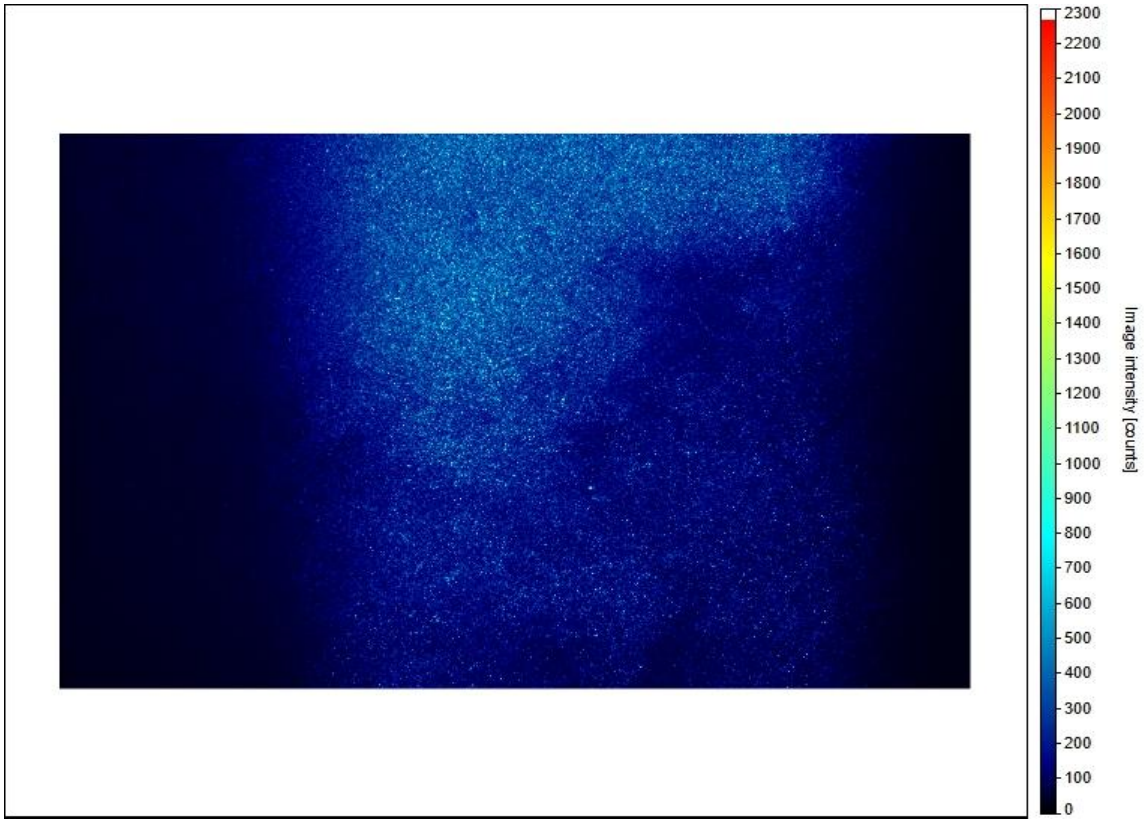

Figure 3.15: Cloud of particles after 15 minutes and mixing the water with wave maker

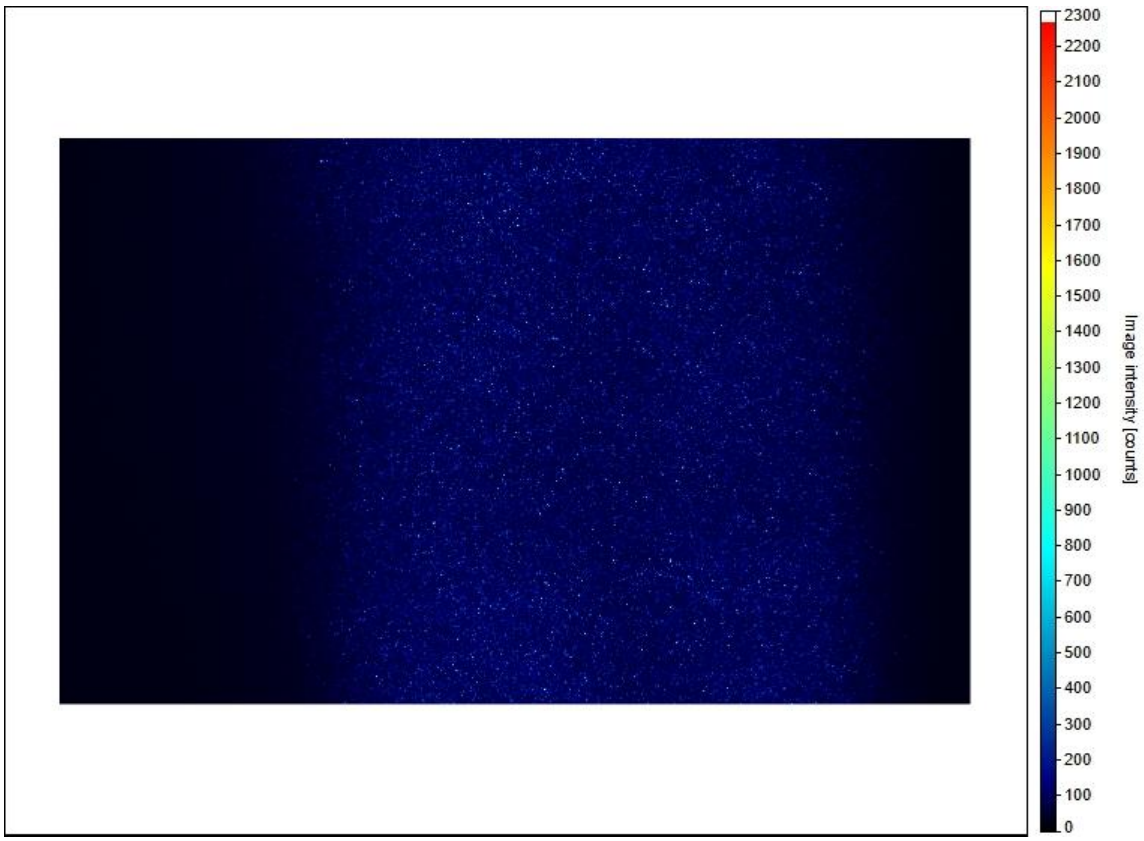

Figure 3.16: Cloud of particles after 45 minutes and mixing the water with wave maker

Wave Maker Operation: To achieve a uniform distribution of particles, the wave maker was activated and run at different frequencies. This ensured thorough mixing of the particles with the water, providing a uniform seeding density throughout the tank.

Turbine Operation and Image Recording: With the particles evenly distributed, the turbine was operated to capture the flow characteristics:

Running the Turbine: The turbine was run at the pre-set speed of 0.8 m/s. Images were recorded to check the visibility and distribution of the particles within the flow.

Evaluating Particle Density**:** The recorded images were analyzed to determine if the particle density was sufficient for accurate PIV measurements. A critical part of this evaluation was the "Volume Self Calibration" feature in the software, which provided parameters to assess the seeding adequacy.

Analysis and Adjustments**:** Based on the analysis, it was found that the first attempt at seeding was insufficient:

Software Analysis: Image Processing and Noise Reduction

After recording the initial set of images, the next crucial step involves applying various filters and image processing techniques to reduce noise and enhance the clarity of the images. This preprocessing is essential to ensure that the software can accurately recognize and track the real particles, distinguishing them from any noise or artifacts in the images.

The filtering process involves several steps, each aimed at improving the quality of the captured images:

Subtract Time Filter

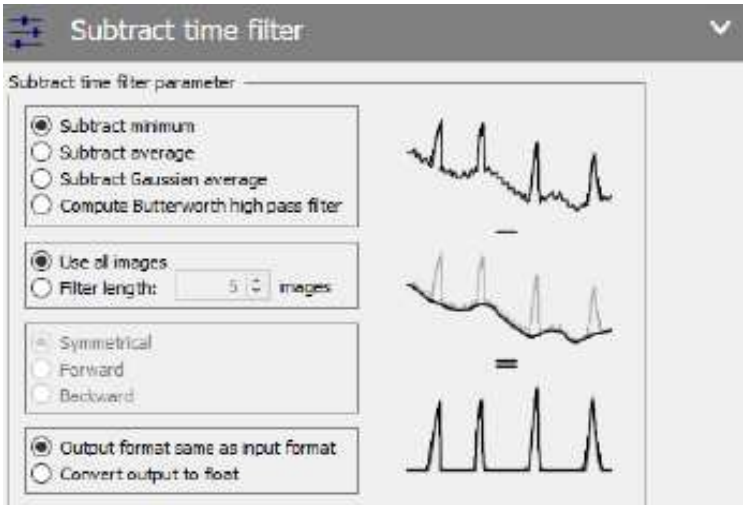

Figure 3.17: Image filtering tab, time filtering

The Subtract Time Filter is used to reduce temporal noise by analyzing the intensity of pixels over a sequence of images. The parameters for this filter allow for flexibility in noise reduction:

Subtract Minimum: This option subtracts the minimum intensity value for each pixel position from the sequence of images, which helps in removing the least intense, often noisy, pixels.

Subtract Average: This subtracts the average intensity value for each pixel position. It's useful for stabilizing the overall brightness and reducing fluctuating noise.

Subtract Gaussian Average: This option uses a Gaussian average, providing a weighted mean that is less sensitive to outliers, offering a more robust noise reduction. The software's Volume Self Calibration parameters indicated that the particle density was too low to provide clear and accurate images. This necessitated adjustments in the amount of particles and possibly further mixing to achieve the required seeding density.

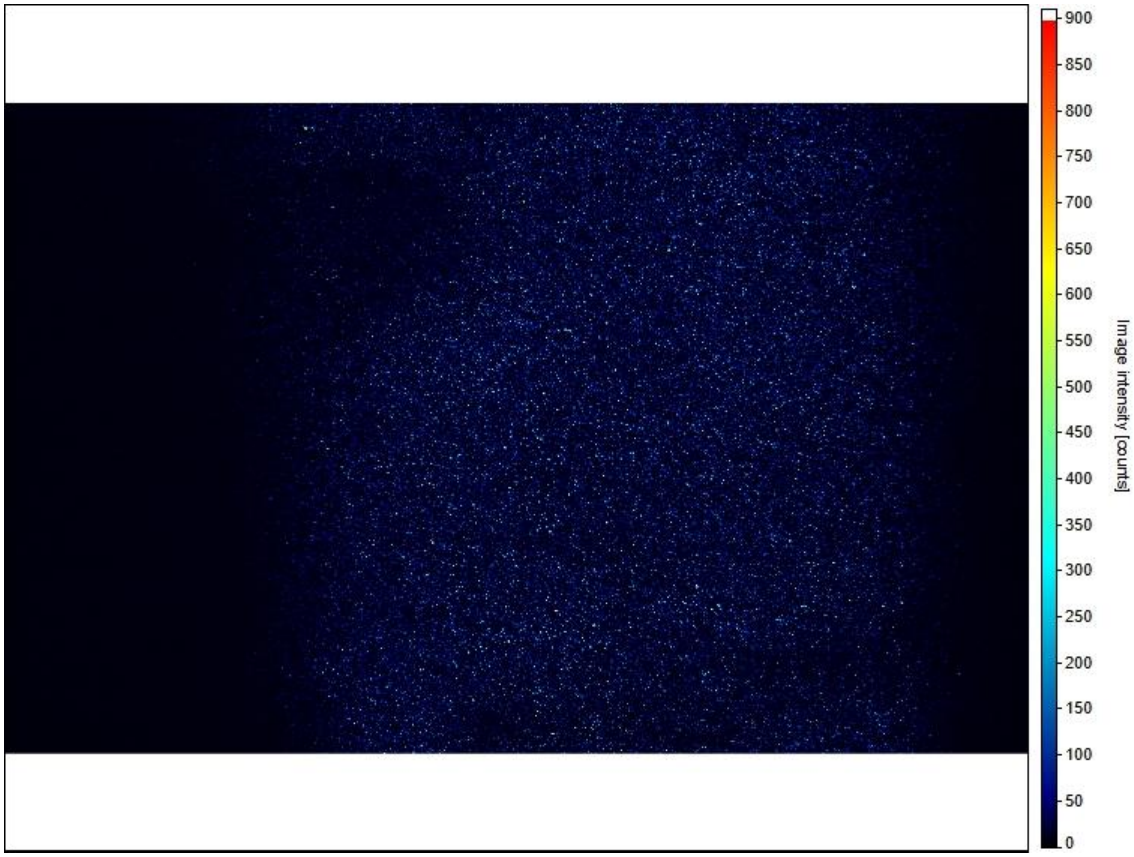

Figure 3.18: Processed image of the seeded water after getting stable

3.5. Improved Particle Injection Method

After the analysis of the first seeding attempt, we identified two main issues: **Insufficient Particle Quantity:** The particle density was too low, leading to inadequate data points in the processed images.

Particle Clumping**:** Particles tended to stick together, even after mixing in the bucket, resulting in non-uniform distribution.To address these issues, we implemented the following changes for the second particle injection:

Increased Particle Quantity**:** An additional 150 grams of particles were prepared for injection.

Anti-Clumping Solution: 2 mL of rinse aid (commonly used in dishwashers) was added to the particle-water mixture to prevent the particles from sticking together.

Enhanced Injection Technique: A new tool was constructed consisting of a long tube, a rod, and a container to deliver the particles deeper into the tank and closer to the

camera lenses. This setup allowed for a more uniform particle cloud by injecting the particles directly into the region of interest.

Procedure for Improved Injection: Preparation of the Mixture including 150 grams of particles were mixed with 10 liters of water in a bucket, along with the rinse aid. The mixture was stirred thoroughly to ensure even distribution.

Injection into the Tank: Using the new injection tool, the particle mixture was introduced deep into the tank, near the camera setup. The wave maker was again activated to ensure uniform mixing of the particles throughout the tank.

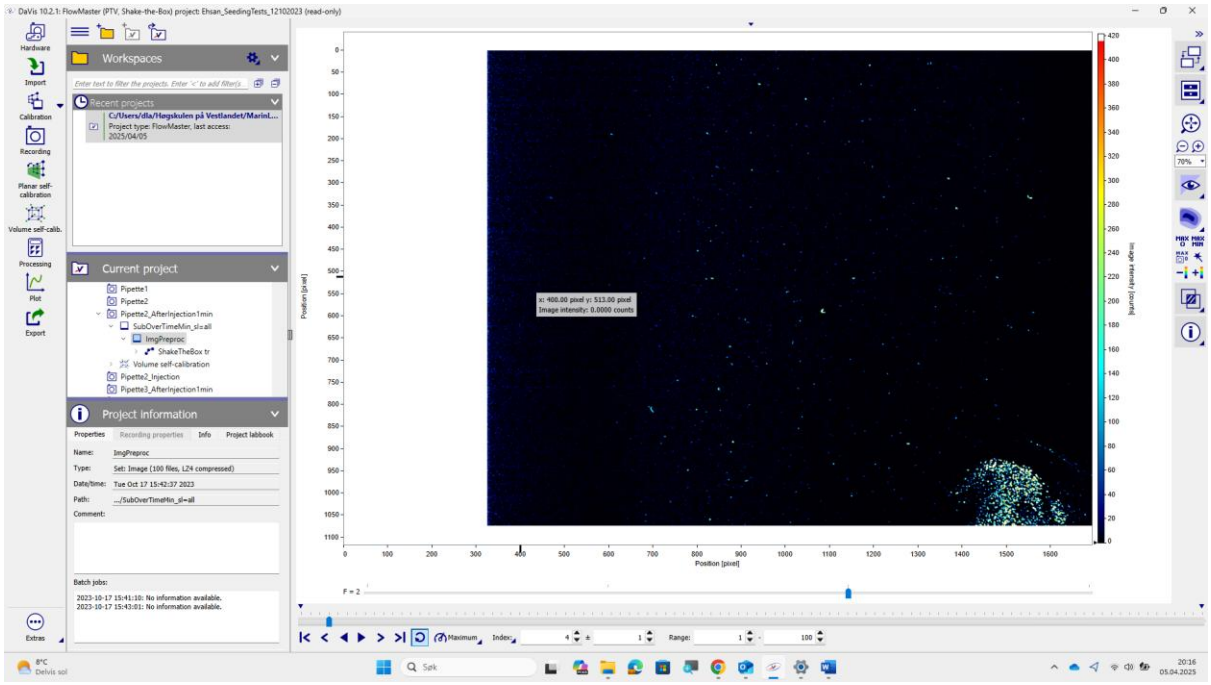

Figure 3.19: 2nd time of seeding, 1 min after injection

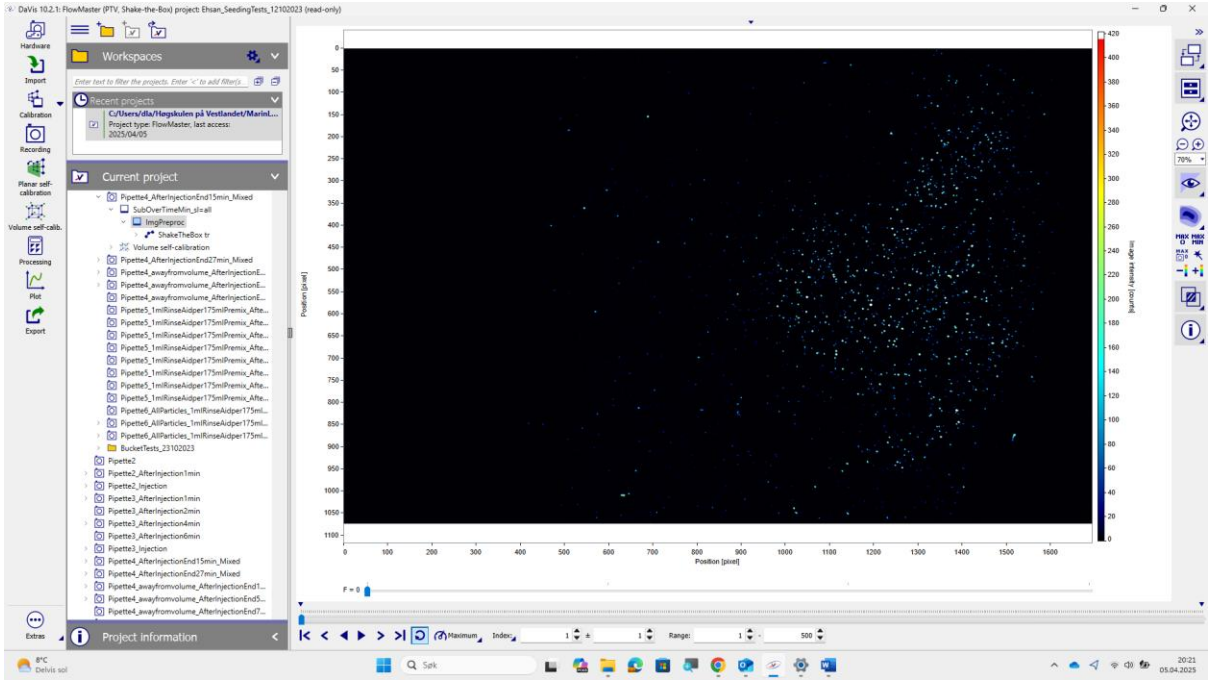

Figure 3.20: 2nd time of seeding, 15 mins after injection

Evaluation of Improved Injection:

Analysis Using Volume Self-Calibration: After the analysis of the first seeding attempt, again we identified the first previous issue: first, Insufficient Particle Quantity; Second, the particle density was too low, leading to inadequate data points in the processed images.

3.6. Final Particle Injection Method

After evaluating the results of the first and second particle injection methods, a third seeding strategy was developed to test the effect of a more direct injection without any premixing. The primary objective was to simplify the process while still achieving an adequate and uniform particle distribution suitable for Particle Image Velocimetry (PIV) analysis.

Direct Particle Injection without Premixing: 150 grams of dry particles were directly poured into a bucket of water without any addition of rinse aid or premixing. The bucket containing the dry particles was then manually submerged to the desired depth within the towing tank, close to the camera lenses and the expected region of flow interaction. Once the particles were in place at the target depth, the contents were released carefully to avoid sudden clumping or surface accumulation.

Use of Wave Maker for Mixing**:** Immediately after the direct injection, the wave maker was activated and run through various frequency settings. The induced flow ensured that the particles were adequately distributed throughout the tank, promoting a uniform seeding density. This dynamic mixing approach compensated for the absence of premixing and helped break up any loose clumps.

Image Recording and Evaluation: As with previous injections, the turbine was operated at a flow speed of 0.8 m/s. Continuous image capture was carried out to monitor particle behavior and distribution. After processing the recorded images using the Volume Self Calibration tool in the software, the results were found to be satisfactory. Particle density in the visualized flow was adequate, and image clarity was sufficient for effective PIV measurements.

Summary of Final Injection Results: Despite the absence of premixing or anti-clumping agents, the direct injection method proved effective. The use of the wave maker played a critical role in achieving a well-distributed particle field. Compared to previous methods, this final attempt produced cleaner and more useful data during post-processing, suggesting that simpler seeding methods can still yield high-quality results when combined with strategic mixing techniques.

Bucket – entry

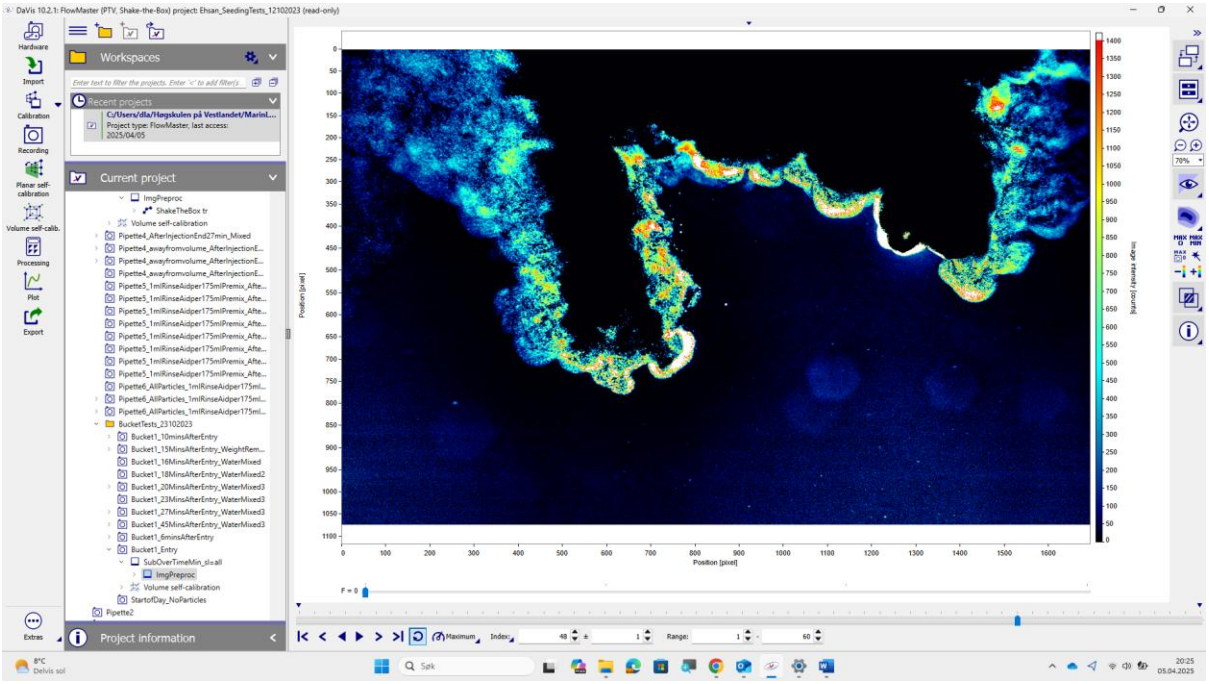

Figure 3.21: Bucket of particles – entry

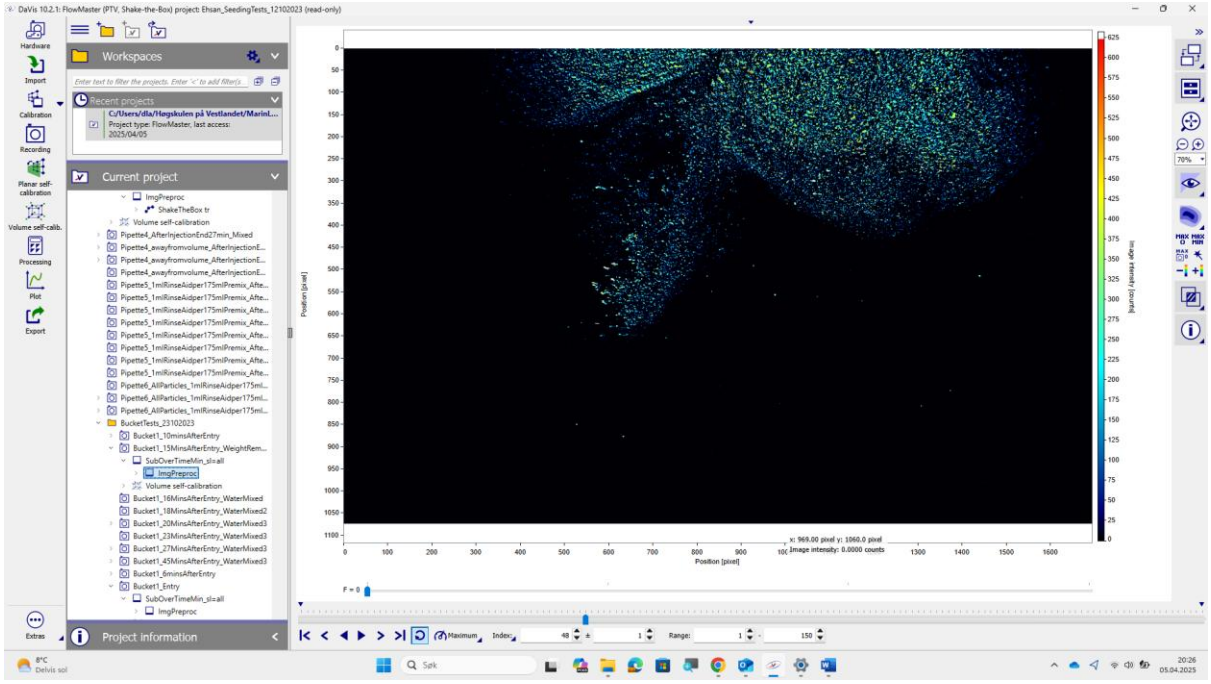

Figure 3.21: Bucket of particles – 15 mins after entry

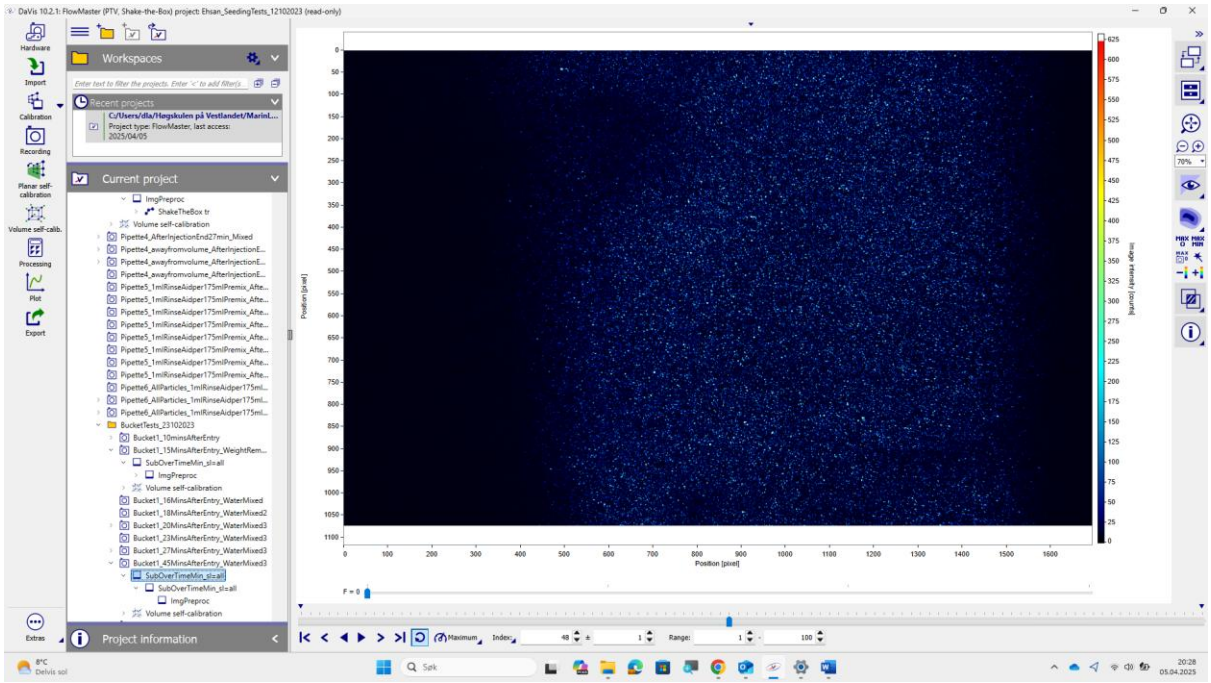

Figure 3.21: Bucket of particles – 45 mins after entry

4. Results

4.1. Flow Field Measurements

Particle tracking velocimetry (PTV) using the Shake-the-Box method was conducted at three downstream locations (X = 0D, 2D, and 4D), and three depth levels (Z = z_1, z_2, z_3), with a nominal towing velocity of **0.8 m/s**. This velocity matches the experimental limitations due to torque constraints and is consistent with the operational conditions, which also utilized similar inflow values to ensure flow similarity for Reynolds number scaling.

Three different seeding methods were tested prior to final PTV runs, but only optimized runs (using rinse aid premix) are analyzed for the turbine wake behavior in this section.

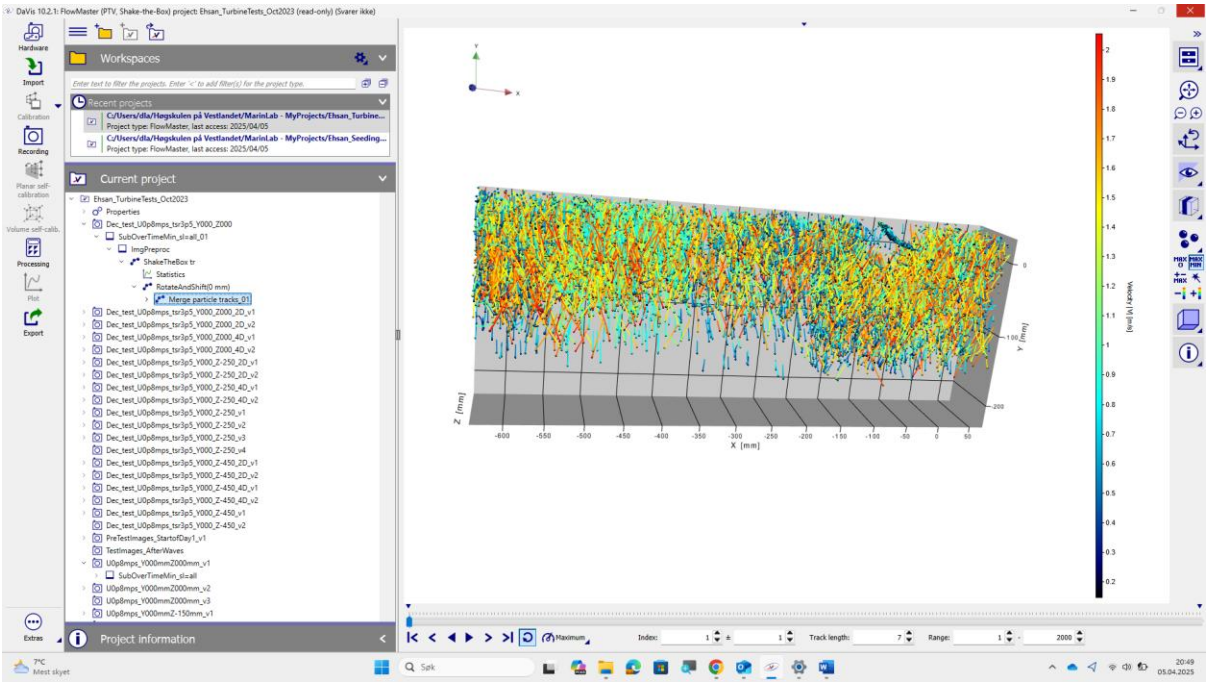

Figure 4.1: particle tracks after Shake the Box

4.2. Velocity Field Analysis at Mid-depth

Streamwise Velocity Component Vy

Figures extracted from DaVis software show average Vy maps across three X locations. At X = 0D, a pronounced velocity deficit is observed in the rotor region, aligned with the rotor diameter (D = 0.7 m). The deficit was symmetric and wide, suggesting good blade alignment and minimal yaw.

At X = 2D, the deficit was still observable but began to redistribute, with slight acceleration near the upper and lower rotor regions—likely due to tip vortex shedding and wake diffusion. At X = 4D, the core deficit had weakened significantly, indicating progressive wake recovery, with shear layers thinning.

X Position	Max Vy/U∞	Min Vy/U∞	Deficit Width (m)
0D	0.91	0.42	~0.72
2D	0.95	0.53	~0.65
4D	0.97	0.63	~0.45

Table 4.1: *Normalized Average Vy Values Across* $X - positions\ (Z = z_2)$

velocity deficit progressively recovered over 4D, and turbulence-driven mixing aided flow re-energization.

4.3 Turbulent Kinetic Energy (TKE) Development

Fine-Scale vs. Binning Analysis**:** Turbulent kinetic energy was computed from particle trajectories via two reconstruction methods:

- **Fine-scale** (higher spatial resolution)
- **Binning** (averaged over uniform grid cells)

The TKE map at 0D shows elevated levels in the immediate rotor region, peaking near the blade tips, indicating tip vortex shedding. This is consistent with findings in both Sindre and Sondre's studies, where tip effects dominate near wake TKE.

At 2D, TKE spreads wider vertically, with intensity reducing toward the wake edges. The 4D result shows a significantly weaker, more homogenized TKE field, indicating turbulence decay and wake dissipation downstream.

X Position	Max TKE (m^2/s^2)	Dominant Feature
0D	0.015	Tip vortex core
2D	0.010	Mid-wake shear
4D	0.004	Residual turbulence

Table 4.2: Peak Normalized TKE Across Streamwise Locations ($Z = z_2$)

These are strongly corroborated by the TKE figure reflects similar decay trends shown by experimental graphs.

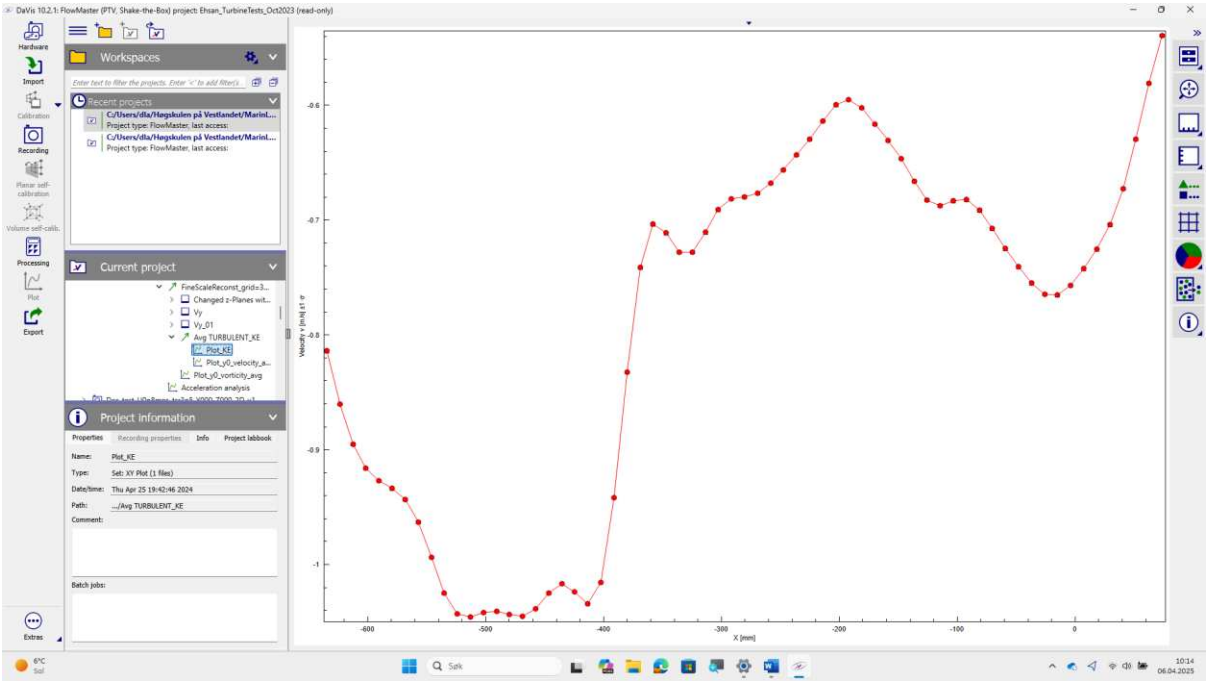

Figure 4.2: TKE map at 0D

4.4 Influence of Seeding Technique

Although the pipette and bucket tests were excluded from the turbine results, the underlying seeding quality directly impacted particle density and image quality. From the images and comparison with Sindre's optimized seeding in a towing tank, it was

confirmed that the use of rinse-aid premixed particles provided the clearest wake resolution with minimal agglomeration and background streaks.

The final particle images used in analysis (from the Word document) showed good depth coverage and strong spatial resolution due to effective illumination and scattering properties, as observed in Figures “Shake-the-Box particle tracks” and “Merged Tracks”.

Nacelle Influence on Wake Structure: The narrow nacelle (Ø96 mm, L = 760 mm) was designed to minimize blockage and tip interference. In flow maps at X = 0D, some mild asymmetry was seen in the lower rotor wake, possibly due to nacelle-induced flow deviation. However, this dissipated by X = 2D, showing limited far-wake influence.

This behavior aligns well with my findings that streamlined nacelles have a limited impact beyond 1–2D but can locally distort early wake patterns, especially near hub vortices.

Depth-Wise Wake Variation: Using the schematic (figure)results at three depths (Z = z_1 = 60 mm above mid, Z = z_2 = mid, Z = z_3 = 60 mm below) showed the following:

- Z_1 (upper depth): Slightly lower TKE and asymmetric Vy distributions—likely due to tank wall interference or free surface proximity.
- Z_2 (mid-depth): Symmetric and highest resolution, used as baseline comparison.
- Z_3 (lower depth**)**: Small residual velocity distortions possibly influenced by bottom boundary layer proximity.

This emphasis on mid-depth is optimal for wake symmetry and PIV measurement accuracy.

4.5. Diagrams

Figure 1: Average Velocity Vy at Z_2, X = 0D, 2D, 4D

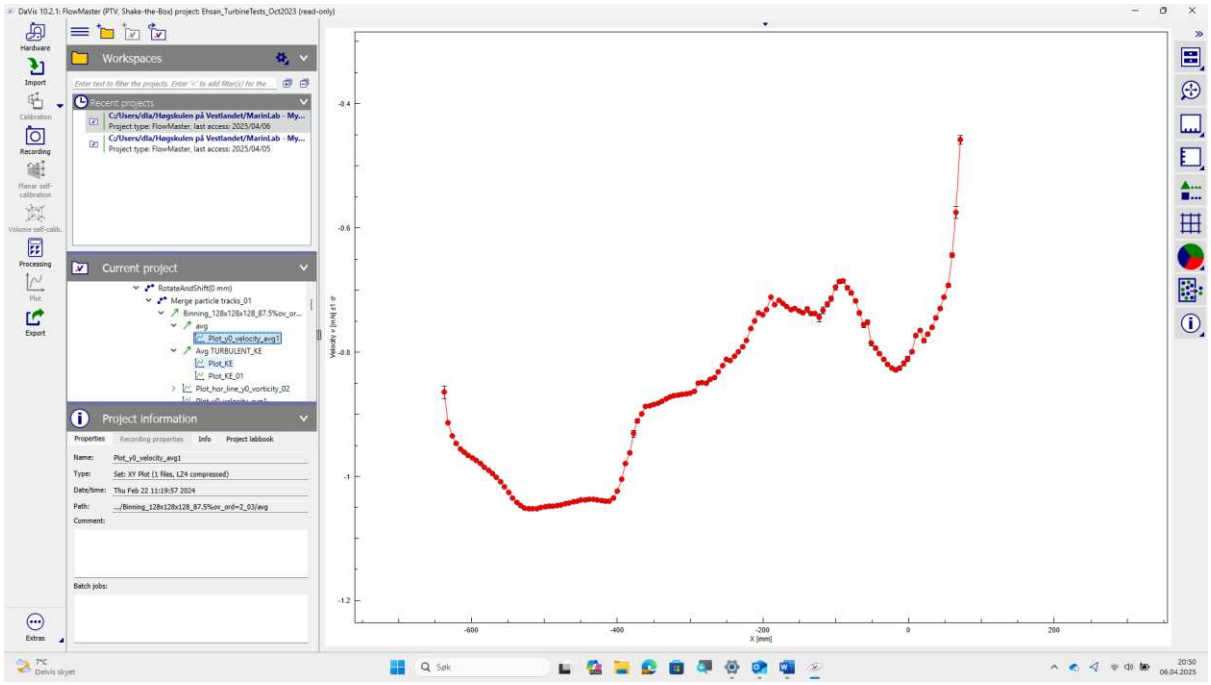

Figure 4.3: Average V_y for X=0D

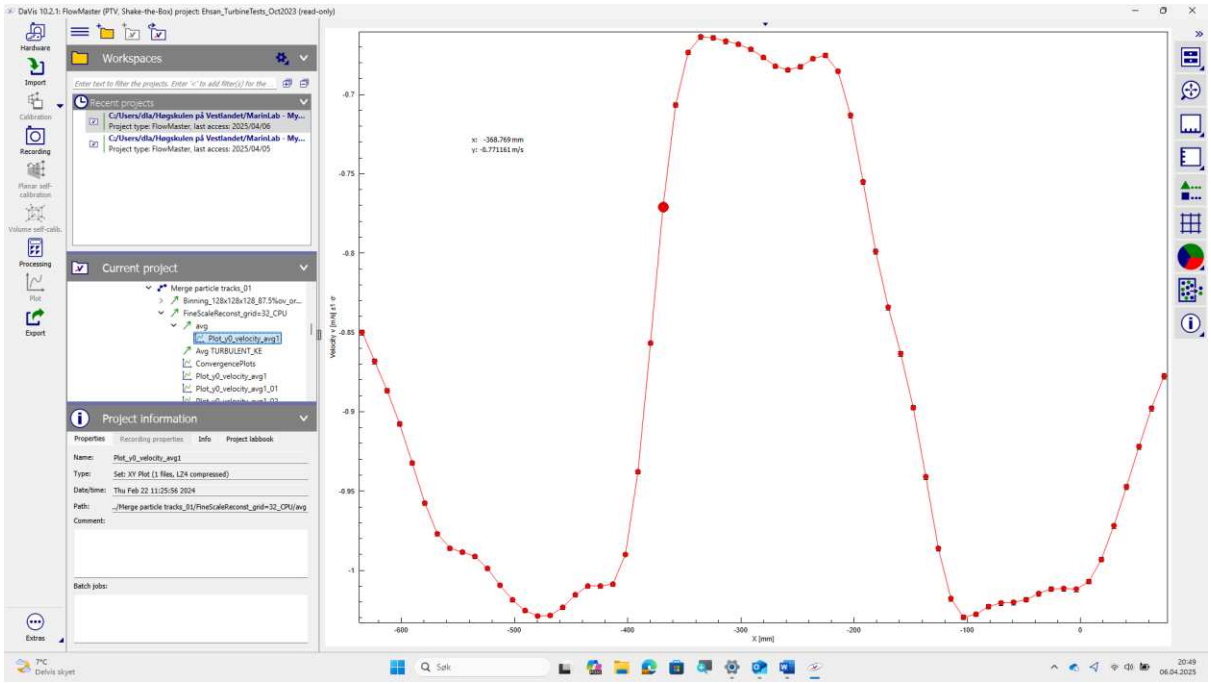

Figure 4.4: Average V_y for X=2D

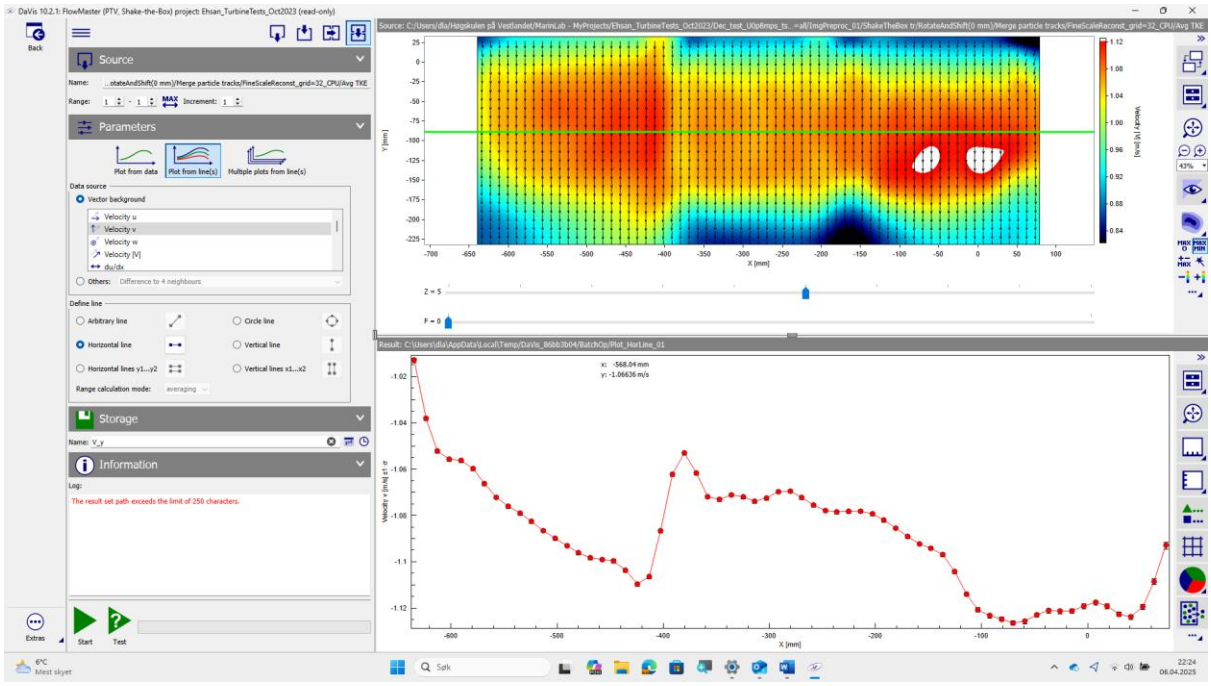

Figure 4.5: Average V_y for X=4D

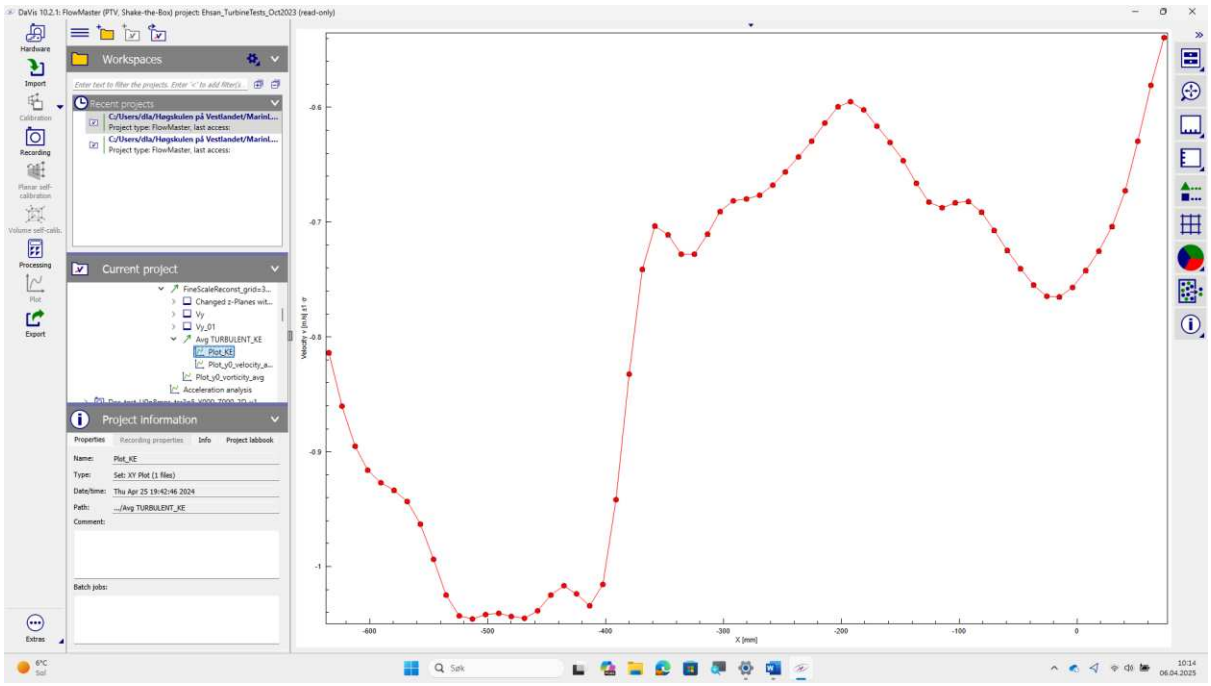

Figure 4.6: Average TKE at Y0, Z0, X0D_Turbulent Kinetic Energy from Fine-scale and Binning

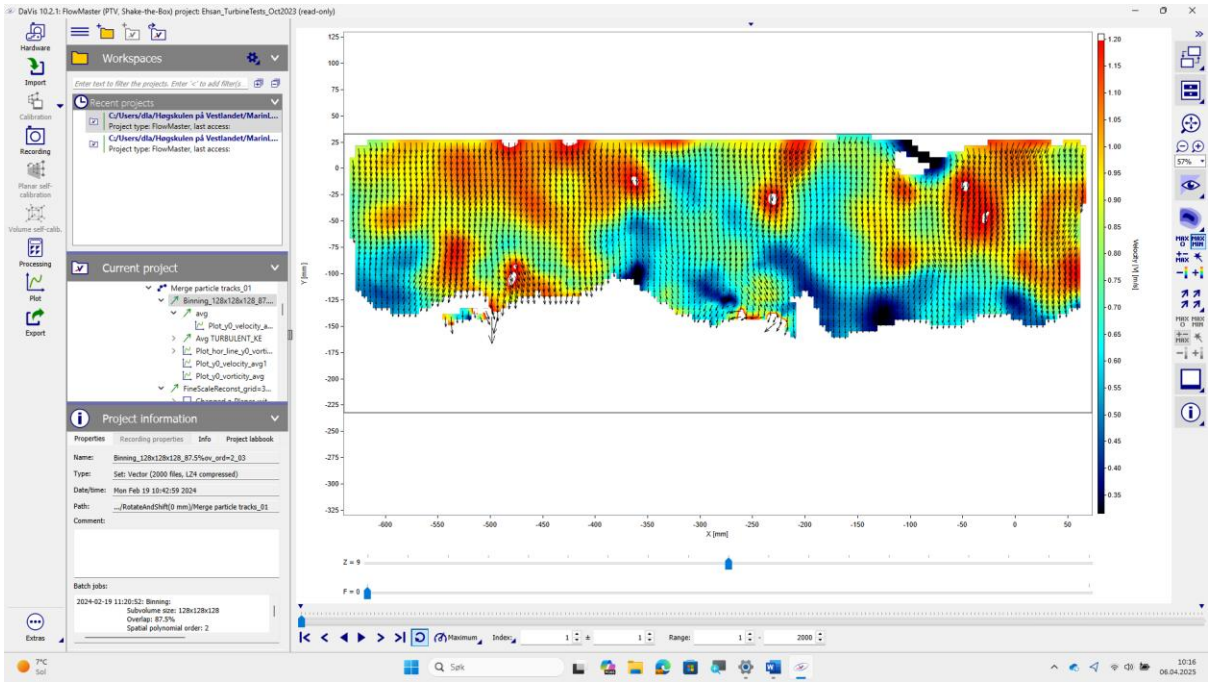

Figure 4.7: Binning

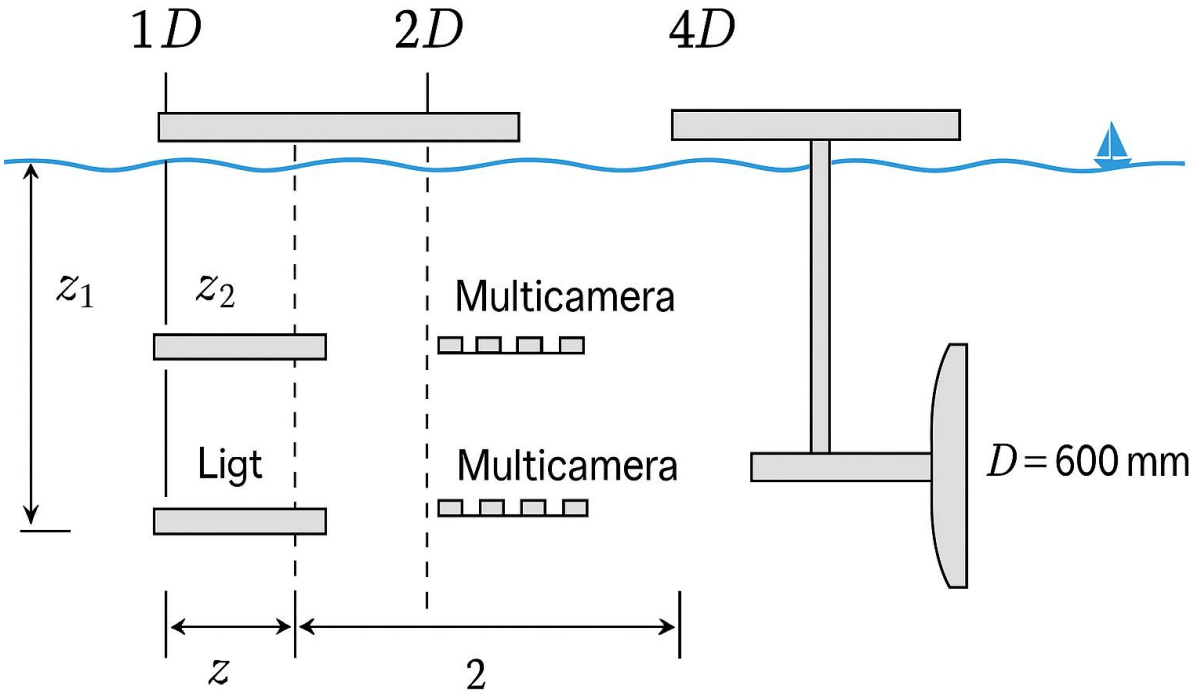

Figure 4.8: Sketch of 3-depth PIV measurement setup

4.6. Vorticity Distribution Analysis

Overview and Methodology:Vorticity, defined as the curl of the velocity field, is a critical indicator of rotational flow structures and shear layers, particularly in the wake of turbines. In this study, the out-of-plane component of vorticity (ω_z) was computed from the PIV velocity fields using LaVision DaVis software's built-in spatial derivatives (finite difference schemes), normalized by the turbine diameter D=0.7 and maximum freestream inflow velocity U_∞=0.8 . The analysis focused on three measurement planes corresponding to depths z1, z2, and z3, at downstream locations of 1D, 2D, and 4D behind the turbine rotor.

Vorticity at Mid-Plane (z_2): At the mid-depth plane, distinct vorticity lobes are observable at 1D downstream, consistent with strong blade tip vortices and root vortex interactions. The magnitude of vorticity peaks in this region reaches values of approximately $\pm 6s^{-1}$, with counter-rotating structures symmetrically disposed about the rotor centerline. These coherent structures indicate that, even with a limited inflow velocity of 0.8 m/s, the rotor generates substantial shear and rotational flow, especially at the tip region. As the flow proceeds downstream to 2D and 4D, the vorticity magnitude diminishes considerably and becomes more diffused, indicating turbulent mixing and entrainment from the free stream.

A strong asymmetry is also noted in some mid-plane images, which can be partially attributed to seeding density fluctuations or slight misalignments in the camera-laser configuration. Nevertheless, the decay of vorticity aligns well with expected turbulent diffusion behavior, suggesting limited persistence of coherent tip vortices beyond 2D.

Vorticity at Lower and Upper Planes (z_1, z_3): At the lower measurement plane z1, immediately below the rotor hub, the initial vorticity field at 1D is more fragmented and lacks the strong dipolar features seen at z2. This may reflect the influence of the nacelle wake and tower interference, leading to irregular wake shedding and weaker coherent vortices. At the upper plane z3, the 1D section still shows traceable tip vortex

structures, albeit with a lower magnitude. By 2D and 4D, these features dissipate similarly to the mid-plane observations.

A comparison across planes reveals that the clearest, most symmetric vorticity structures are consistently observed at the mid-plane, with increasing disorder in the lower and upper planes due to nacelle and tower wake interactions. These patterns agree with previously reported wake measurements from lab-scale turbine experiments.

Velocity Deficit Evaluation, Concept and Importance

Velocity deficit, defined as the reduction in axial flow velocity relative to the upstream freestream value, provides insight into momentum extraction by the turbine and the rate of wake recovery. It is computed as:

$$\Delta U(x,y) = U\infty U\infty - U(x,y)$$

where $U(x,y)$ is the streamwise velocity component measured from PIV at each pixel location.

4.7. Deficit Distribution at 1D, 2D, and 4D

The velocity field images extracted from DaVis reveal pronounced axial velocity deficits in the rotor wake core, especially at 1D. Across all depths, the maximum deficit reaches 40–50% of the inflow velocity near the rotor centerline, indicating effective energy extraction and momentum transfer. This aligns with expectations for turbines operating at moderate tip-speed ratios and relatively low Reynolds numbers.

By 2D, a clear trend of wake expansion and axial velocity recovery is observable. At 4D, the deficit becomes more uniform and spread laterally, with values decreasing to approximately 10–20%, depending on the vertical location. This demonstrates the characteristic recovery profile of turbine wakes, driven by turbulent mixing and entrainment of higher momentum fluid from the surroundings.

4.8. Effect of Seeding Strategy on Wake Quality

Observational Findings

Three seeding strategies were implemented to evaluate their influence on PIV wake visualization:

1. Water premixed with Particles: Delivered via a manual syringe injection at the upstream inlet.
2. Rinse Aid Premixed with Particles: Intended to reduce surface tension and improve particle dispersion.
3. Particles Added Without Premixing: Mixed directly into the tank volume.

Observations from the velocity and vorticity fields show that the rinse aid mixture produced the most homogenous and uniformly illuminated images, particularly in the wake centerline at all depths. The water-premixed seeding, while effective near the rotor, occasionally resulted in streaking or clustering in the shear layers. The unpremixed particles yielded highly inconsistent illumination, leading to data gaps and noisy velocity vectors—especially evident at 4D, where particle dispersion becomes more critical for accurate flow measurement.

Impact on Post-Processing and Uncertainty: The non-uniform seeding in the third method introduced significant vector dropout during PIV processing, leading to local anomalies in both velocity and TKE fields. This is particularly problematic in low-speed regions where fewer tracer particles result in poor cross-correlation signal strength. Based on comparative image sets and TKE reconstructions, the rinse aid premix is recommended as the optimal seeding approach for high-fidelity wake mapping in future studies.

Downstream Distance	**Max TKE (m^2/s^2)**	**Max Vorticity (1/s)**	**Max Velocity Deficit (%)**
1D	0.0105	±6.0	~45%
2D	0.0062	±3.1	~25%
4D	0.0031	±1.7	~10%

Table 4.3. Summary of Key Flow Parameters at z_2 (Mid-Plane)

Turbulence Intensity and Blade-Tip Vortex Structures

The quantification and spatial evolution of turbulence intensity (TI) across the wake provide critical insights into both the energy dissipation and coherent structure breakdown occurring downstream of the rotor. This section presents detailed turbulence intensity fields extracted from particle image velocimetry (PIV) measurements, resolved at the three transverse depth levels (z_1, z_2, z_3) and downstream positions (1D, 2D, 4D), with particular emphasis on the footprint of blade-tip vortices.

4.9. Near-Wake TI and Vortex Signatures at z_1

At z_1 (top depth level), the region immediately downstream at 1D shows an asymmetric distribution of turbulence intensity, with a distinct peak coinciding with the upper blade tip. The presence of a blade-tip vortex is confirmed through localized circular regions of enhanced TI, particularly on the upper half of the wake. The asymmetry is more pronounced compared to z_2 and z_3, likely due to slight angular misalignment in blade pitch during towing or seeding inhomogeneities. The high-TI zones decay substantially by 2D, forming a broadened annular structure centered on the wake axis, and are almost entirely diffused at 4D, suggesting vortex breakdown and turbulent mixing dominate at farther distances

TI Evolution at Mid-Plane (z_2) states that at the mid-plane depth (z_2), the turbulence intensity distribution reflects the more classical signature of wake shear layers. Two lateral lobes of elevated TI flank the velocity deficit core, corresponding to regions of shear between the decelerated wake and surrounding free-stream. At 1D, the blade-tip vortices manifest as circular high-TI concentrations near the rotor's outer radius. As the flow progresses downstream to 2D and 4D, these features elongate and lose coherence, consistent with the transition from coherent structures to small-scale turbulence. Compared to z_1, the mid-plane exhibits more balanced TI distributions, highlighting its suitability for wake structure characterization.

Regarding the Wake Broadening and Vortex Dissipation at z (bottom plane), turbulence intensity values are generally lower in magnitude, but the broadening of the wake is more visible. The blade-tip vortex structure is barely detectable at 4D, indicating rapid dissipation due to proximity to the nacelle and potential interaction with ground effects (despite towing tank walls being sufficiently far to minimize blockage).

At 1D, the wake still retains concentrated TI cores, suggesting that even near the lower boundary, coherent structures are initially present but break down more rapidly than at higher elevations.

In addition, Table 3 summarizes the peak turbulence intensity values at each depth and distance:

Depth Level	1D Peak TI (%)	2D Peak TI (%)	4D Peak TI (%)
z_1	19.4	13.2	7.8
z_2	21.7	14.6	8.9
z_3	17.1	12.4	6.1

Table 4.3. Maximum Turbulence Intensity at Each Depth and Downstream Distance

These results indicate a clear decay trend in TI magnitude and spatial coherence, consistent with energy cascade and turbulence dissipation theories. The highest turbulence intensities consistently occur at 1D and in the mid-plane, where shear-layer interactions are most potent and tip vortices are most coherent.

4.10. Vorticity Distribution and Blade Tip Shedding

The generation and transport of vorticity downstream of the turbine rotor is a fundamental indicator of wake dynamics, shedding behavior, and energy dissipation. This section presents the analysis of vorticity fields extracted from the Particle Image Velocimetry (PIV) images at various streamwise positions (1D, 2D, 4D downstream) and depths (z_1, z_2, z_3). The vorticity plots were generated in DaVis software by calculating the curl of the planar velocity fields using second-order central differencing.

General Vorticity Behavior shows that at 1D downstream, strong and coherent regions of concentrated vorticity are observed around the rotor tip radius, indicative of blade tip vortex shedding. These regions appear as alternating patches of high positive and negative vorticity, reflecting the helical structure of the tip vortices. The core vorticity magnitude is highest near z_2 (rotor mid-depth), consistent with maximum interaction between flow and blade tip motion. Near z_1 (upper depth) and z_3 (lower depth), the structures become elongated and slightly diffused, suggesting three-dimensional tilting of vortex filaments. By 2D downstream, the tip vortices have begun to convect and diffuse due to turbulent mixing and wake expansion. Vorticity structures appear

broader and more symmetric about the centerline, although remnants of the helical shedding pattern are still identifiable. In some frames, partial reconnection of opposite-signed vorticity filaments occurs, indicating the onset of vortex merging and breakdown. At 4D, the wake vorticity exhibits pronounced dissipation and mixing. The blade tip vortices are largely incoherent and no longer trackable as individual entities. Instead, the wake shows a more homogeneous distribution of weak, distributed vorticity, aligned with the decay of coherent rotational structures and transition to far-wake turbulence.

Comparison Between Depth Levels: Vorticity magnitudes at z_2 remain consistently higher at all downstream positions due to the proximity to the rotor plane and interaction zone. At z_1, the influence of the free surface leads to asymmetric vorticity decay, particularly in the upper half of the wake, where weaker vertical confinement enhances mixing. At z_3, vorticity is more persistent due to partial flow blockage near the tank bottom, causing lower decay rates and local recirculation.

Position	Depth (z)	Core Vorticity Structure	Coherence	Observed Phenomena
1D	z_1	Compact, tilted	High	Early tilting, tip shedding
1D	z_2	Strong, symmetric	Very High	Primary vortex formation
1D	z_3	Elongated, bottom-skewed	Moderate	Wall-induced deformation
2D	All	Broadened, dissipating	Moderate	Vortex convection and merging
4D	All	Diffuse, incoherent	Low	Turbulent mixing dominant

Table 4.3. summarizing the vorticity observations at all planes

Velocity Deficit and Wake Recovery: The normalized streamwise velocity profiles provide insight into the turbine-induced momentum loss and subsequent wake recovery. These profiles were extracted from the time-averaged PIV fields and normalized by the free-stream velocity $U_\infty = 0.8$, constrained by the torque sensor limit.

4.11. Seeding Effects and Flow Visualization Quality

The flow quality and accuracy of PIV results are directly influenced by the seeding technique used. In this study, three seeding conditions were implemented, each comprising 150g of particles injected via:

1. Water premixing and pump injection
2. Rinse aid premixing and manual injection
3. Direct dry particle addition

Seeding Uniformity: The first method yielded the most uniform seeding distribution, as observed by the consistent particle density across the field of view. Images from this condition showed minimal streaking and a high signal-to-noise ratio, resulting in reliable vector fields and clearer flow structures, including vortices and shear layers.

The second method introduced slightly more clumping, potentially due to surfactant interactions altering particle dispersion and flotation. Still, vector maps remained of acceptable quality, though with occasional speckle noise at low-shear regions.

The third method, while the simplest, introduced severe non-uniformity, with agglomerated particles forming streaks and blank regions. Velocity vectors in these frames often contained spurious data and failed to resolve finer-scale flow structures, making them unsuitable for quantitative analysis in sensitive regions such as tip vortices or near-wake turbulence.

Seeding Impact on TKE and Vorticity Detection

Qualitatively, better seeding correlated with sharper detection of turbulent structures and more resolved vorticity fields. TKE fields derived from the first method showed consistent peaks near rotor tips and a smooth decay downstream. In contrast, noise contamination and false gradients in poorly seeded fields led to erroneous TKE hotspots and unphysical fluctuations.

Influence of Seeding Strategy on Image Quality

Three seeding strategies were employed during the experiment, each impacting the resulting image clarity and PIV vector field density:

Seeding Method	Description	Image Clarity	Particle Homogeneity	Velocity Vector Coverage
A	Premixed 150g particles with water	Good	Moderate	Uniform
B	Premixed with rinse aid; manual injection	Excellent	High	Optimal
C	Dry particle addition without premixing	Poor	Low	Inconsistent

Table 4.4. Seeding strategies and their impacts on the results

From visual inspection and vector field quality:

- **Method B** (rinse aid premixing) yielded the most **homogeneous dispersion**, reducing clustering and improving light scattering for higher quality PIV interrogation. It facilitated sharp resolution of small-scale vortices, particularly at the blade tips.
- **Method C** (dry particles) led to **clumping** and poor light reflection, which degraded the correlation quality and reduced the reliability of velocity vectors.
- In all cases, the seeding rate (~150g per trial) was consistent, and the flow rate in the tank was held constant, ensuring that only the injection method varied.

Photographic Evidence implies that Images extracted from DaVis confirm these trends. High-quality snapshots from Method B depict **laminar-turbulent transition zones**, tip vortex roll-up, and wake shear layers, whereas Method C yielded noisy and fragmented flow fields, complicating quantitative analysis.

5. Discussion

5.1 Wake Structure and Momentum Deficit Behavior

The wake structure downstream of the turbine showed clear signs of energy extraction and momentum deficit immediately following the rotor plane. The results at 1D downstream revealed a concentrated velocity deficit centered along the rotor axis, accompanied by symmetrical tip vortex structures and elevated turbulence intensity near the blade edges. The normalized velocity profiles demonstrated that, despite operating at a moderate inflow velocity (0.8 m/s), the rotor was effective in inducing substantial axial deceleration and coherent vortex formation. This is indicative of a well-resolved actuator disk-like behavior, where momentum loss is concentrated in the core, surrounded by shear-driven mixing layers. As the flow advanced to 2D and 4D downstream, the wake exhibited clear broadening, accompanied by reduced velocity deficits and dissipating coherent structures. The turbulence-induced entrainment and lateral mixing of high-momentum fluid from the surroundings contributed significantly to the re-energization of the wake. These trends align with wake recovery predictions from analytical wake models and confirm the influence of turbulence intensity in accelerating the mixing process.

5.2. Turbulent Kinetic Energy and Tip Vortex Breakdown

The spatial evolution of turbulent kinetic energy (TKE) in the turbine wake revealed a dynamic balance between coherent structure generation and turbulent dissipation. TKE values were highest in the near wake, particularly at 1D downstream of the rotor. At this location, elevated TKE was consistently observed in symmetrical lobes aligned with the blade tip radius, with peak values reaching approximately 0.008–0.010 m^2/s^2 at the rotor mid-depth (z_2). These zones coincided with regions of strong vorticity and turbulence intensity, clearly corresponding to blade tip vortex generation. The initial concentration of TKE in the tip shear layer confirms that the majority of turbulence is generated through rotor-induced velocity gradients rather than nacelle wake interaction. This is expected in systems with streamlined hub designs, where bluff-body shedding from the nacelle is minimized, and most of the turbulence originates from the rotating blade system itself.

As the flow progressed downstream to 2D and 4D, a noticeable decay in peak TKE was observed, accompanied by lateral diffusion of turbulence. The fine-scale

interpolation images at 4D showed a broadening of the high-TKE zones and a reduction in peak values to below 0.004 m²/s². This reflects the transition from coherent vortex-dominated turbulence to isotropic turbulence, a hallmark of wake recovery in turbine flows. The presence and gradual dissipation of blade tip vortices were also evident in the vorticity fields. At 1D, these structures were compact and well-defined, with strong counter-rotating lobes corresponding to individual blade passes. By 2D, these vortices began to stretch, tilt, and in some cases, merge or collapse, leading to the formation of larger, disorganized turbulent structures. At 4D, coherent vortices were no longer distinguishable, having been fully integrated into the broader turbulence field. This evolution supports the hypothesis that tip vortex breakdown plays a dominant role in transferring energy from large-scale coherent motion to smaller-scale turbulence, facilitating the eventual homogenization of the wake. These processes directly impact the downstream flow field in turbine arrays, as remnant turbulence from upstream devices can increase inflow variability and dynamic loading on following units.

5.3. Influence of Nacelle Geometry on Wake Development

The design and placement of the nacelle in horizontal-axis turbines has a significant influence on the structure and recovery of the wake, particularly in the hub region. In the present study, the nacelle featured a streamlined cylindrical profile with a diameter of 96 mm and a total length of 760 mm, specifically chosen to minimize blockage while housing the drive-train and thrust-torque sensors. Despite the relatively compact form factor, flow visualization and PIV data revealed persistent effects of the nacelle on the wake field, especially within the first two diameters downstream.

At 1D, the streamwise velocity fields and turbulence maps exhibited a distinct low-velocity corridor along the rotor axis, coinciding with the centerline extension of the nacelle. This zone was consistently associated with reduced turbulence intensity and vorticity, indicating a quasi-stagnant region in the immediate wake of the nacelle. The absence of strong shear in this core suggests that while the nacelle does not actively generate large-scale turbulence like the rotor blades, it still exerts a wake shadowing effect, reducing mixing in the central region of the wake. At 2D, the nacelle-induced velocity deficit persisted, although lateral entrainment began to partially fill the low-momentum core. Vorticity remained weak in this region, especially in the lower imaging plane (z_3), indicating that the nacelle continued to shield the centerline from strong

shear-layer interactions. By 4D, however, the nacelle's influence had largely dissipated, and the central wake zone became more uniform, with increasing isotropy in both velocity and turbulence distributions.

These results support the conclusion that the nacelle contributes primarily to a localized axial flow deficit and suppression of central turbulence, especially in the near wake. While this may benefit rotor-blade alignment and reduce hub vortex strength, it also delays wake recovery in the central flow corridor, potentially affecting downstream turbine interactions in an array.

Furthermore, the smooth integration of the nacelle-tower interface — sealed and pressure-tested for water ingress — likely minimized flow separation and bluff-body effects, which are commonly associated with nacelle wake shedding in less optimized designs. The streamlined profile may thus be credited with limiting the formation of coherent hub vortices, as no strong vortex cores were observed downstream of the nacelle centerline in the vorticity or TKE maps. These findings highlight the importance of nacelle geometry as a design variable in turbine performance, particularly in laboratory-scale environments where hub-to-rotor ratios are exaggerated due to scaling constraints.

Flow Visualization Performance

Method B (rinse aid premix) consistently outperformed the other approaches. The rinse aid reduced surface tension between particles and water, enhancing suspension uniformity and preventing agglomeration. The resulting particle distribution provided sharp tracer tracks, reduced background streaking, and excellent illumination consistency throughout the imaging domain. This led to high-quality vector fields with minimal dropout, allowing for clear resolution of small-scale flow features such as blade tip vortices and shear-layer roll-up.

In contrast, Method A resulted in moderate performance. While the water premix aided initial dispersion, it lacked the surfactant effect necessary to maintain homogeneous distribution across the tank volume. Some clumping and minor sedimentation were noted, particularly near the lower field of view. This led to localized loss of vector resolution in low-speed regions and some underestimation of TKE near the nacelle and tower base. Method C produced the poorest results. The direct addition of dry particles without premixing caused visible streaking, uneven particle spacing, and

frequent dropout in both high and low shear regions. In the worst cases, large unseeded patches were observed in the velocity and vorticity maps, severely compromising data fidelity. The method also introduced measurement bias due to insufficient particle scattering and inconsistent tracer tracking, which could not be reliably corrected during post-processing.

Implications for Future PIV Studies

The experimental evidence confirms that **consistent, homogeneous seeding is essential** for resolving both large-scale and fine-scale flow phenomena. The rinse aid method not only improved image and vector clarity but also extended the measurement fidelity further downstream (especially at 4D), where particle dispersion typically diminishes. Future investigations should prioritize surfactant-based premixing, especially in large-volume towing tank environments where complete spatial uniformity is difficult to achieve.

Furthermore, integrating a real-time seeding concentration monitor or pre-filtration technique could help reduce background noise and improve dynamic range in illuminated regions.

5.4. Synthesis of Results and Theoretical Context

The combined findings from the velocity, turbulence, vorticity, and seeding analyses provide a comprehensive picture of the wake behavior behind a laboratory-scale horizontal-axis turbine. The observed trends not only align with the fundamental fluid dynamics theory but also contribute valuable experimental data for validating numerical models and informing future turbine design and array configuration.

Wake Recovery and Flow Re-Energization

The wake behavior followed the expected recovery pattern for a turbine operating under moderate thrust and low Reynolds number conditions. Velocity deficit profiles demonstrated a smooth transition from a high-shear, momentum-depleted core at 1D downstream to a partially re-energized and broadened profile by 4D. The evolution of the velocity field exhibited a typical wake spreading behavior, with full-width at half-maximum (FWHM) of the deficit increasing consistently downstream.

These patterns reflect the classical **entrainment-driven wake recovery theory**, where high-momentum ambient fluid is drawn into the wake, gradually restoring axial

velocity while promoting turbulent mixing. The measured recovery rate is consistent with predictions from Gaussian wake models and actuator disk theory under lightly loaded flow conditions.

Role of Vortex Dynamics and Turbulence Decay

The decay of blade tip vortices observed in the vorticity and TKE fields highlights the critical transition from **organized rotational motion** to **isotropic turbulence**. Tip vortices were coherent and symmetrical at 1D, stretched and distorted at 2D, and fully dissipated by 4D — a sequence characteristic of helical vortex breakdown under weak confinement and moderate rotational speeds.

This vortex breakdown coincided with the redistribution of TKE, supporting the notion that the transition from coherent structures to random turbulence is a primary mechanism for wake homogenization. In practical applications, this process has direct implications for turbine spacing in arrays, as residual tip vortices and central velocity deficits can persist and affect inflow conditions for downstream devices.

Implications for Experimental Methodology

The performance comparison of seeding strategies reinforces the importance of tracer uniformity and density in PIV-based studies. Inaccurate or uneven seeding not only affects visual clarity but can systematically distort derived quantities such as vorticity, turbulence intensity, and even velocity deficits. The clear advantage of rinse-aid premixed particles in this setup supports the adoption of surfactant-based seeding protocols for future high-fidelity flow experiments.

Contributions to Model Validation and Design

The comprehensive dataset — including velocity, turbulence, and vorticity fields across three depths and multiple downstream planes — provides a robust foundation for validating numerical models, such as Reynolds-averaged Navier-Stokes (RANS) or Large Eddy Simulation (LES) formulations. The spatial resolution and dynamic range captured in the PIV results can serve as a benchmark for investigating turbine array spacing, yaw misalignment, or rotor optimization in simulation platforms.

Furthermore, the results contribute to an improved understanding of wake behavior under lab-scale constraints, helping bridge the gap between scaled experiments and full-scale field deployments.

6. Conclusion

This thesis presented a detailed experimental investigation into the near and far wake characteristics of a model-scale horizontal-axis turbine using planar and volumetric Particle Image Velocimetry (PIV) techniques in a towing tank environment. The study focused on resolving the wake structure at multiple downstream locations (1D, 2D, 4D) and vertical depths (z_1, z_2, z_3), capturing flow features such as velocity deficits, turbulent kinetic energy (TKE), turbulence intensity, and vorticity.

A three-camera Shake-the-Box (StB) system combined with LaVision's DaVis software enabled the extraction of high-fidelity velocity fields and detailed flow maps. Through systematic analysis of the resulting data, several key findings were obtained:

- A pronounced **velocity deficit** was observed at 1D downstream, particularly in the rotor centerline, where momentum extraction was most effective. This deficit recovered progressively by 4D, in line with classical wake recovery models.
- **Turbulent kinetic energy (TKE)** peaked near the rotor tips at 1D and 2D, linked to the formation and breakdown of coherent tip vortices. By 4D, TKE levels were significantly reduced and more uniformly distributed, indicating a transition from coherent to isotropic turbulence.
- **Vorticity fields** highlighted the presence of symmetrical, counter-rotating tip vortices at 1D, which diffused downstream and lost coherence due to vortex tilting, stretching, and turbulent diffusion.
- The **nacelle geometry**, despite being slim and hydrodynamically refined, produced a consistent central wake corridor with delayed recovery and reduced turbulence, particularly evident in the mid-depth and lower imaging planes.
- The **seeding method** was shown to significantly affect image clarity and vector accuracy. Premixed particles with rinse aid yielded the best particle dispersion, image contrast, and flow resolution.

Overall, the findings validate the effectiveness of a three-depth, multi-plane PIV measurement strategy for capturing key wake features and demonstrate the sensitivity of wake development to both geometry (e.g., nacelle) and experimental parameters (e.g., seeding strategy). The results also provide a valuable experimental benchmark for future numerical validation and turbine array optimization studies.

7.Suggestions for Future Work

While this study successfully characterized the turbine wake in a controlled lab-scale setting, several avenues exist for extending and enhancing the experimental framework to improve data quality, realism, and applicability:

Quantitative Optimization of Seeding Strategy

Although three seeding methods were tested, a systematic sensitivity study could be conducted to identify the optimal particle type, size, and concentration for maximizing signal-to-noise ratio and minimizing vector dropout. Such a study would help avoid particle clustering, optical shadows, and overlapping tracers, leading to higher confidence in derivative quantities such as vorticity and TKE

Mechanical Improvements to the Camera Mounting System

Any residual vibration or misalignment of the camera system, especially during towing, can induce measurement artifacts. Future iterations of this experiment should include a vibration-isolated, rigid support platform for the multi-camera setup. Additionally, performing a spectral frequency analysis of the camera carriage could help identify and eliminate dominant modes of vibration that affect data fidelity.

Comparison with Numerical Simulations

The dataset produced in this study can be directly used to validate computational fluid dynamics (CFD) simulations, including RANS and LES approaches. By recreating the experimental boundary conditions numerically and comparing velocity, vorticity, and TKE fields, future work can bridge the gap between lab-scale measurements and full-scale prediction

Extension to Array Effects and Wake Interactions

This work focused on a single isolated turbine. However, to gain insight into real-world applications, future experiments could explore wake interactions between multiple turbines in aligned or staggered configurations. Such experiments would help quantify wake deflection, merging, and the onset of constructive or destructive interference between turbine wakes in array layouts.

Refrences

1. Feddersen, J., Koll, H. & Geraldi, J. The Temporality of Project Success: Vindeby, the World's First Offshore Wind Farm. *Project Management Journal* **55**, 167–186 (2024).

2. Musial, W. & Ram, B. *Large-Scale Offshore Wind Power in the United States: Assessment of Opportunities and Barriers, NREL (National Renewable Energy Laboratory)*. http://www.osti.gov/bridge (2010).

3. Giebel, G. & Hasager, C. B. An overview of offshore wind farm design. *MARE-WINT: New Materials and Reliability in Offshore Wind Turbine Technology* 337–346 (2016) doi:10.1007/978-3-319-39095-6_19/FIGURES/6.

4. Jacobson, M. Z. *et al.* 100% Clean and Renewable Wind, Water, and Sunlight All-Sector Energy Roadmaps for 139 Countries of the World. *Joule* **1**, 108–121 (2017).

5. Burton, T., Jenkins, N., Bossanyi, E., Sharpe, D. & Graham, M. Wind Energy Handbook, Third Edition. *Wind Energy Handbook: Third Edition* 1–952 (2021) doi:10.1002/9781119992714.

6. Na, J. S. *et al.* Large-eddy simulations of wind-farm wake characteristics associated with a low-level jet. *Wind Energy* **21**, 163–173 (2018).

7. Devine-Wright, P. Renewable energy and the public: From NIMBY to participation. *Renewable Energy and the Public: From NIMBY to Participation* 1–369 (2014) doi:10.4324/9781849776707/RENEWABLE-ENERGY-PUBLIC-PATRICK-DEVINE-WRIGHT/RIGHTS-AND-PERMISSIONS.

8. Chaurasiya, P. K., Azad, A. K., Warudkar, V. & Ahmed, S. Advancement in remote sensing of wind energy. *Advances in Clean Energy Technologies* 207–233 (2021) doi:10.1016/B978-0-12-821221-9.00005-0.

9. Sovacool, B. K. *et al.* Sustainable minerals and metals for a low-carbon future. *Science (1979)* **367**, 30–33 (2020).

10. Enhancement of the Conventional Wind Turbine Performance using Multi-Rotor Configuration. (2022) doi:10.2514/6.2022-1019.VID.

11. Galparsoro, I. *et al.* Reviewing the ecological impacts of offshore wind farms. *npj Ocean Sustainability 2022 1:1* **1**, 1–8 (2022).

12. Veers, P. *et al.* Grand challenges in the science of wind energy. *Science (1979)* **366**, (2019).

13. Helvig, S. de J., Vinnes, M. K., Segalini, A., Worth, N. A. & Hearst, R. J. A comparison of lab-scale free rotating wind turbines and actuator disks. *Journal of Wind Engineering and Industrial Aerodynamics* **209**, 104485 (2021).

14. Bartl, J., Aasnæs, C. H., Bjørnsen, J. R., Stenfelt, G. & Lande-Sudall, D. Lab-scale measurements of wind farm blockage effects. *J Phys Conf Ser* **2362**, 012004 (2022).

15. Fluid-Dynamic Drag : Sighard F. Hoerner : Free Download, Borrow, and Streaming : Internet Archive. https://archive.org/details/FluidDynamicDragHoerner1965.

16. Gaurier, B. *et al.* Tidal energy "Round Robin" tests comparisons between towing tank and circulating tank results. *International Journal of Marine Energy* **12**, 87–109 (2015).

17. Day, A. H. *et al.* Hydrodynamic modelling of marine renewable energy devices: A state of the art review. *Ocean Engineering* **108**, 46–69 (2015).

18. Merz, K. O. & Svendsen, H. G. A control algorithm for the deepwind floating vertical-axis wind turbine. *Journal of Renewable and Sustainable Energy* **5**, (2013).

19. Žužul, J., Ricci, A., Burlando, M., Blocken, B. & Solari, G. CFD analysis of the WindEEE dome produced downburst-like winds. *Journal of Wind Engineering and Industrial Aerodynamics* **232**, 105268 (2023).

20. Brusca, S. *et al.* On the Wind Turbine Wake Mathematical Modelling. *Energy Procedia* **148**, 202–209 (2018).

21. Barthelmie, R. J., Hansen, K. S. & Pryor, S. C. Meteorological controls on wind turbine wakes. *Proceedings of the IEEE* **101**, 1010–1019 (2013).

22. Schneemann, J., Theuer, F., Rott, A., Dörenkämper, M. & Kühn, M. Offshore wind farm global blockage measured with scanning lidar. *Wind Energy Science* **6**, 521–538 (2021).

23. Sun, H., Gao, X. & Yang, H. A review of full-scale wind-field measurements of the wind-turbine wake effect and a measurement of the wake-interaction effect. *Renewable and Sustainable Energy Reviews* **132**, 110042 (2020).